Journal of Peridynamics and Nonlocal Modeling
https://doi.org/10.1007/s42102-020-00038-7

REVIEWS

A Review of Local-to-Nonlocal Coupling Methods in Nonlocal Diffusion and Nonlocal Mechanics

Marta D'Elia[1] · Xingjie Li[2] · Pablo Seleson[3] · Xiaochuan Tian[4] · Yue Yu[5]

Received: 16 December 2019 / Accepted: 17 July 2020 / Published online: 30 November 2021

Abstract

Local-to-nonlocal (LtN) coupling refers to a class of methods aimed at combining nonlocal and local modeling descriptions of a given system into a unified coupled representation. This allows to consolidate the accuracy of nonlocal models with the computational expediency of their local counterparts, while often simultaneously removing nonlocal modeling issues such as surface effects. The number and variety of proposed LtN coupling approaches have significantly grown in recent years, yet the field of LtN coupling continues to grow and still has open challenges. This review provides an overview of the state of the art of LtN coupling in the context of nonlocal diffusion and nonlocal mechanics, specifically peridynamics. We present a classification of LtN coupling methods and discuss common features and challenges. The goal of this review is not to provide a preferred way to address LtN coupling but to present a broad perspective of the field, which would serve as guidance for practitioners

✉ Pablo Seleson
selesonpd@ornl.gov

Marta D'Elia
mdelia@sandia.gov

Xingjie Li
xli47@uncc.edu

Xiaochuan Tian
xctian@ucsd.edu

Yue Yu
yuy214@lehigh.edu

[1] Department of Quantitative Modeling & Analysis, Sandia National Laboratories, Livermore, CA 94550, USA

[2] Department of Mathematics and Statistics, University of North Carolina at Charlotte, Charlotte, NC 28223, USA

[3] Computer Science and Mathematics Division, Oak Ridge National Laboratory, Oak Ridge, TN 37831, USA

[4] Department of Mathematics, University of California, La Jolla, San Diego, CA 92093, USA

[5] Department of Mathematics, Lehigh University, Bethlehem, PA 18015, USA

in the selection of appropriate LtN coupling methods based on the characteristics and needs of the problem under consideration.

Keywords Nonlocal models · Coupling methods · Nonlocal diffusion · Nonlocal mechanics · Peridynamics

1 Introduction

1.1 Nonlocal Models and the Need of Coupling Methods

Nonlocal models such as nonlocal diffusion and peridynamics can describe phenomena not well represented by classical partial differential equations (PDEs). These include problems characterized by long-range interactions and discontinuities [20, Chapter 1]. For instance, in the context of diffusion, long-range interactions effectively describe anomalous diffusion, whereas in the context of mechanics, crack formation results in material discontinuities. We refer to these phenomena, in a general sense, as *nonlocal effects*. Even though this work is focused on nonlocal models for diffusion and mechanics in single-physics applications, nonlocal models can characterize a wide range of complex scientific and engineering problems, including subsurface transport [18, 76, 77, 116, 117], phase transitions [11, 30, 33], image processing [24, 36, 63, 89], multi-scale systems [3, 4, 51, 123], turbulence [10, 108, 115], and stochastic processes [26, 37, 94, 98].

The fundamental difference between the nonlocal models considered in this paper and classical local PDE-based models is the fact that the latter only involve differential operators, whereas the former also rely on integral operators.[1] The integral form allows for the description of long-range interactions (spanning either small regions or the whole space) and reduces the regularity requirements on problem solutions. Here, we consider nonlocal models, based on integro-differential formulations, characterized by spatial integral operators that lack spatial derivatives. This enhances the accuracy of their modeling representations by generalizing the space of admissible solutions, which can feature discontinuities.

Despite their improved accuracy, the usability of nonlocal equations could be compromised by several modeling and numerical challenges such as the unconventional prescription of nonlocal boundary conditions, the calibration of nonlocal model parameters, often unknown or subject to uncertainty, and the expensive numerical solution. In fact, the computational cost of solving a nonlocal problem is significantly higher than that corresponding to PDEs. Specifically, the associated computational expense of a nonlocal problem depends on the ratio between the characteristic nonlocal interaction length (the so-called interaction radius or *horizon*) and the chosen simulation grid or mesh size. When this ratio becomes large, simulations can be unfeasible [20, Chapter 14].

Nevertheless, it is often the case that nonlocal effects are concentrated only in some parts of the domain, whereas, in the remaining parts, the system can be accurately described by a PDE. The goal of local-to-nonlocal (LtN) coupling is to combine the computational efficiency of PDEs with the accuracy of nonlocal models, under the assumption that the

[1] Nonlocal models, in general, can be based on *weakly nonlocal* or *strongly nonlocal* formulations. The former enrich classical PDEs by explicitly including higher gradients of field variables, whereas the latter are based on integral-type formulations with a weighted average of field variables [13, 41, 75]. In this paper, we only concern ourselves with strongly nonlocal formulations.

location of nonlocal effects can be identified. In this context, the main challenge of a coupling method is to accurately merge substantially different local and nonlocal descriptions of a single system into a mathematically and physically consistent coupled formulation.

As an added value, LtN coupling can provide a viable way to circumvent the non-trivial task of prescribing nonlocal boundary conditions. Such conditions have to be prescribed in a layer surrounding the domain where data are not available or are hard to access; however, surface (local) data are normally available. In practice, this requires extending surface (local) boundary conditions to volumetric (nonlocal) boundary conditions in a way that is not always clear or well-defined. An ad hoc treatment of nonlocal boundaries often results in unphysical surface effects (see discussions in [80]). Using a local model adjacent to the boundary of the domain allows for prescription of classical boundary conditions, provided the solution around the boundary is regular enough. Throughout this paper, we mention coupling approaches that have been used for this task. There are other potential benefits of LtN coupling, such as controlling undesired wave dispersion or leveraging available computational tools based on classical PDEs. However, these are beyond the scope of this paper.

The purpose of this paper is to present the state of the art of LtN coupling in the context of nonlocal diffusion and nonlocal mechanics, specifically peridynamics. While the list of proposed LtN coupling methods is extensive, this paper focuses on a select number of approaches. The description provided should, however, give the reader a broad enough perspective on the diversity of LtN coupling techniques and the variety of ways to approach LtN coupling problems, both in terms of mathematical formulation and practical implementation. We stress that our goal is strictly to give an overview of available coupling strategies and highlight their properties, while describing common features and challenges. This work does not intend to present a relative assessment of LtN coupling methods. Yet the reader can use this review as a guide for selecting the most appropriate method for the problem at hand.

1.2 Overview of Classes of Coupling Methods

We divide coupling approaches in two main classes based on how the transition from a nonlocal description to a local description is carried out. A schematic overview of such classification and of the methods belonging to each class is reported in Fig. 1; that figure also indicates the corresponding sections where the methods are described in detail. We refer to the first class as the *Constant Horizon* (CH) class, which contains approaches characterized by an abrupt change in the horizon as we move from the nonlocal region to the local region; whereas we refer to the second class as the *Varying Horizon* (VH) class, which contains approaches that, in contrast, feature a smooth transition of the horizon. In the next paragraphs we briefly mention several methods belonging to each class. A detailed description of those methods will be reported in the next sections.

In the CH class, we identify a first group of approaches that resemble generalized domain decomposition (GDD) methods. A first example is the optimization-based coupling method introduced in [34], analyzed in [35], and extended in [39]. This strategy treats the coupling condition as an optimization objective, which is minimized subject to the model equations acting independently in their respective sub-domains. As opposed to other LtN coupling approaches, this method reverses the roles of the coupling conditions and the governing equations, keeping the latter separate. In particular, the coupling of local and nonlocal models is effected by couching the LtN coupling into an optimization problem. The objective is to minimize the mismatch of the local and nonlocal solutions on the overlap of their sub-domains, the constraints are the associated governing equations, and the controls are

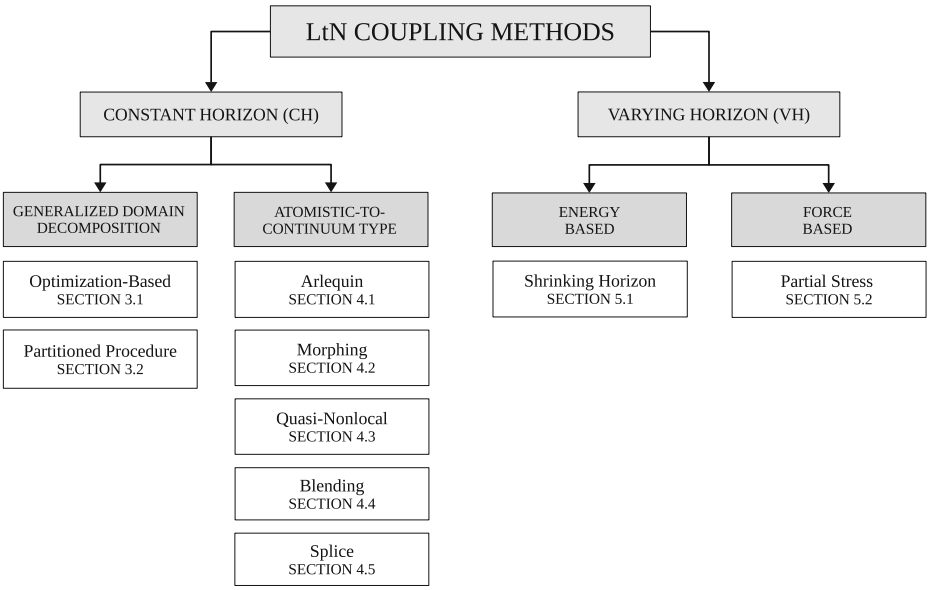

Fig. 1 Overview of classes of LtN coupling approaches and corresponding methods

the nonlocal and local boundary conditions on the virtual boundaries generated by the decomposition.

A second GDD example relies on the partitioned procedure as a general coupling strategy for heterogeneous systems, such as multi-scale and multi-physics problems [8, 93, 112, 146]. In the partitioned procedure, the system is divided into sub-problems in their respective sub-domains. Different models are then employed independently in each sub-problem, which communicates with other sub-problems only via transmission conditions on the sub-domain interfaces. The coupled problem is then solved based on iterative solutions of sub-problems, and proper transmission conditions are required on the sub-domain interfaces to impose solution continuity on those interfaces and to enforce the energy balance of the whole system. Among the possible transmission conditions, the Robin transmission condition, which is a linear combination of the Dirichlet and Neumann transmission conditions, has been proven to be very efficient (see, e.g., [8, 31, 46, 48]). In [158], a partitioned procedure with Robin transmission conditions was applied to LtN coupling of mechanics models with an overlapping region, and the method was later extended to LtN coupling without an overlapping region in [157].

A second group of approaches in the CH class is also based on a decomposition of the domain, which normally resembles an overlapping domain decomposition. However, as opposed to GDD methods, these approaches typically rely on hybrid descriptions that combine local and nonlocal models in a transition region between local and nonlocal sub-domains. We refer to this group of approaches as atomistic-to-continuum (AtC) type coupling approaches due to their resemblance to such coupling methods (see, e.g., the review articles [32, 91, 100]). We observe that, in some sense, AtC coupling is a special case of LtN coupling, where the nonlocal model is a discrete atomistic representation and the local model is given by a classical PDE.

In the group of AtC type coupling approaches, a first example is the Arlequin method. This is a general coupling technique introduced in [14, 15] and further studied in [16, 17].

This technique was applied to AtC coupling in [12] with various follow-on works (see, e.g., [29, 110, 111]). Application of the Arlequin method for LtN coupling was proposed in [71] in the context of static problems and later applied to dynamic settings in [149]. The Arlequin method is an example of an energy-based blending approach, where the energy of the system in the transition region is defined as a weighted average of the local and nonlocal energies. In the local and nonlocal sub-domains, the energy is defined according to the models operating in those sub-domains. A Lagrange multiplier enforces compatibility of the kinematics of both models.

A second example of AtC type coupling is the morphing approach proposed in [90] and extended in [5, 6, 72]. This method is based on blending the material properties of the local and nonlocal models. The method consists of a single model defined over the entire domain with an equilibrium equation that contains both local and nonlocal contributions. The transition between the nonlocal sub-domain and the local sub-domain is achieved through a gradual change in the material properties characterizing the two models in the transition region or "morphing" zone. In this region, local and nonlocal material properties are suitably weighted under the constraint of energy equivalence for homogeneous deformations.

A third example of AtC type coupling is the quasi-nonlocal (QNL) coupling method. This method was originally proposed in the context of AtC coupling [127] and is based on energy minimization with the aim of eliminating spurious forces for linear deformations. The QNL method redefines the nonlocal energy of the system by reformulating nonlocal interactions not fully contained within the nonlocal sub-domain. The QNL strategy was applied to nonlocal-to-nonlocal coupling in [82] and to LtN coupling in [56].

A fourth example of AtC type coupling is the force-based blending method proposed in [118] and extended in [121]. Force-based blending has been studied in the context of AtC coupling (see, e.g., [7, 57, 83, 84]). This approach employs a blending function to create a weighted average of the local and nonlocal governing equations, and that function is chosen in a way that the blended model reduces to the local and nonlocal models in their respective sub-domains. Similar to the morphing approach, a single blended model is defined over the entire domain; however, the force-based blending method does not enforce energy equivalence. In this paper, we employ the term "blending" to refer to force-based blending, since other methods which could be classified within a blending category, such as the Arlequin and morphing, are called by their specific names. As opposed to AtC blending methods, which normally seek means to blend given atomistic and continuum models, the peculiarity of the LtN blending method from [118, 121] is that a reference nonlocal model is first postulated over the entire domain, and then the blended model is attained by simply combining the use of a blending function with assumptions on the material response. An underlying connection between the local and nonlocal models is leveraged in the derivation of the blended model. A force-based coupling approach, which resembles blending due to a partition of unity-based superposition of local and nonlocal parts of displacements within an overlapping region, was presented in [137] and extended in [138].

A final example of AtC type coupling is the splice method. This method was first proposed in [132] to couple two nonlocal models with different horizons and then applied to LtN coupling. A similar approach for LtN coupling, although introduced instead for discretized models, was presented in a series of publications (see [58, 102, 128–130, 151, 159, 160]) and combined with a VH technique, which will be introduced below, in [161]. In the splice method, the governing equation at each point is given by either the local or nonlocal model. There is no particular coupling enforced, except that points described by the nonlocal model may interact with points described by the local model and vice versa. When such

a situation occurs, points with a given description (either local or nonlocal) treat their environment, e.g., the nonlocal neighborhood, with the same modeling representation as their own. For instance, a point in a nonlocal region interacting with some points in a local region would treat those points as if they were also described by a nonlocal model.

In the VH class, we can also find energy-based and force-based approaches. The idea behind VH is that a nonlocal model converges to a local model, under suitable regularity assumptions, when the horizon approaches zero (see Sections 2.2.1 and 2.2.2). Naturally, allowing the horizon to vary spatially in a domain, so that it approaches zero in certain sub-domains with enough regularity, provides a transition from a nonlocal to a local representation. Discussions on a VH in the context of adaptive refinement appeared in [21, 22] and similar adaptivity ideas appeared in the context of atomistic systems in [119] to remove surface effects. A nonlocal formulation with spatially varying horizon applied to interface problems was presented in [120], where two-horizon systems were treated and specialized to the case in which one of the two horizons is taken to zero. A similar formulation applied to two- or multi-horizon systems was discussed in [73, 113, 114, 123]. More recently, in [28], for a two-horizon setting, the coupling problem was formulated via minimization of the total energy of the system; the LtN coupling problem can be obtained by taking the limit to zero of one of the horizons. The case of a smoothly varying horizon was presented and analyzed in [132], and it was used to couple two nonlocal models with different horizons. In [140, 144], the validity of nonlocal models with a shrinking horizon applied to LtN coupling was discussed. An approach using a VH for LtN coupling of discretized models was discussed in [104].

The group of energy-based approaches in the VH class is related to the formulations presented in [113, 120, 123, 132, 140, 144]. Such energy-based formulations, unfortunately, introduce linear spurious forces. In order to allow varying the horizon in space while preventing this coupling artifact, the partial stress method was presented in [132]. This method belongs to the group of force-based approaches and introduces a new tensor referred to as the partial stress, which is used to describe the material response in the transition region between the nonlocal and local sub-domains.

There are alternative approaches in the literature that address LtN coupling. Specifically, while we focus on LtN coupling of continuum models, some proposed methods tackle the coupling problem at the discrete level (we have already mentioned a few above). The first peridynamic work in this context appears in [92], where a coupling is performed by implementing a peridynamic model in a conventional finite element (FE) analysis code using truss elements; a similar work can be found in [125]. In this context, an overlapping-based approach between peridynamics and classical FEs, which relies on interfacial elements, is described in [78, 88, 154], whereas a sub-modeling approach is presented in [1, 107]. Efforts to couple peridynamics with the extended finite element method (FEM) appear in [47, 62, 87]. A coupling approach with an emphasis on balancing the forces between the peridynamic region and the FE region to satisfy Newton's third law is proposed in [155]. Another coupling method based on coarsening a peridynamic discretization is proposed in [123] and implemented in [152, 153]; these implementations resemble the splice method in the context of FE discretizations of peridynamic models. Finally, works addressing dynamic coupling artifacts, such as interfacial spurious wave reflections, can be found in [61, 79, 103]. All these approaches, however, are beyond the discussions held in this review.

Desired Properties of a LtN Coupling Method There are various considerations to account for when designing a LtN coupling method. The first one is ensuring that the reference local and nonlocal models are *physically consistent*. This is guaranteed by the convergence

of the nonlocal model to the local model as discussed in Sections 2.2.1 and 2.2.2 for nonlocal diffusion and nonlocal mechanics, respectively. Once the local and nonlocal models are determined to be physically consistent, the main challenge becomes removing or minimizing the appearance of coupling artifacts on the interface/in the transition region between the local and nonlocal sub-domains. We describe below some desired properties of LtN coupling methods and discuss related coupling artifacts.

A basic desired property of a LtN coupling method is *patch-test consistency*, which is established when such a method passes the so-called patch test or consistency test [86, 91, 100]. The main idea is as follows: if for a certain class of problems the local and nonlocal solutions, u^l and u^{nl}, respectively, coincide, then "patching" the two problems by coupling the corresponding models should still return the same problem solution. Note that to be comparable, the local and nonlocal problems are augmented with consistent boundary conditions and forcing terms.

As an example, we define a linear patch test in one dimension as follows:

Definition 1 (**Linear patch test**) Given a linear function $u^{\text{lin}}(x) = a_0 + a_1 x$ with a_0 and a_1 constants and local and nonlocal operators $\mathcal{L}^{\text{L}}$ and $\mathcal{L}^{\text{NL}}$, respectively, such that

$$\mathcal{L}^{\text{L}} u^{\text{lin}} = 0 \quad \text{and} \quad \mathcal{L}^{\text{NL}} u^{\text{lin}} = 0,$$

a coupling method passes the linear patch test if, in the absence of a forcing term and with consistent boundary conditions, u^{lin} is also the solution of the coupled problem.

Note that patch tests in higher dimensions can be defined in a similar manner. Also, similar to Definition 1, one can define a higher-order patch test as follows:

Definition 2 (**Higher-order patch test**) Given a polynomial of degree $p \in \{2, 3\}$, $u^{\text{poly}}(x) = \sum_{i=0}^{p} a_i x^i$ with $\{a_i\}_{i=0}^{p}$ constants, and local and nonlocal operators such that

$$\mathcal{L}^{\text{L}} u^{\text{poly}} = f^{\text{poly}} \quad \text{and} \quad \mathcal{L}^{\text{NL}} u^{\text{poly}} = f^{\text{poly}},$$

where f^{poly} is a polynomial of degree $p-2$, a coupling method passes the pth-order patch test if, with consistent boundary conditions and forcing term given by f^{poly}, u^{poly} is the solution of the coupled problem.

Examples of linear ($p=1$) and quadratic ($p=2$) patch tests are provided in the following sections. Note that the linear patch test is the most popular consistency test used in many coupling settings; however, it is rather simple as often higher orders of deformation occur in practical scenarios. To illustrate such an example, we include a quadratic patch test.

A related concept to the patch test is that of "ghost" forces. Specifically, when a coupling method does not pass a patch test, non-physical forces normally arise in the transition region between the local and nonlocal sub-domains. These non-physical forces are often referred to as "ghost" forces and can be computed as the residual of the equilibrium equation (see, e.g., [90]). The concept of "ghost" forces was introduced in the context of AtC coupling (see, e.g., [100]).

Another desired property of a LtN coupling method is *asymptotic compatibility*. This ensures that the method preserves the physical consistency of the local and nonlocal models. Specifically, the solution corresponding to a LtN coupling method should be such that it coincides with the local solution everywhere when the nonlocal effects vanish. More details in this regard are provided in the following sections.

A third desired property of a LtN coupling method is *energy equivalence*. Due to the physical consistency of the local and nonlocal models, it is expected that these models would have equivalent energy descriptions for a certain class of problems. Consequently,

an appealing property of a LtN coupling method is to also preserve the energy description for such class of problems. This consideration becomes a natural requirement for energy-based LtN coupling methods, since they possess an associated energy functional. In contrast, force-based LtN coupling methods do not possess, in general, an associated energy functional.

While the above properties concern common coupling artifacts in static problems, other spurious effects can emerge in dynamic scenarios. A prime example of these spurious effects is wave reflections on the interface/in the transition region between the local and nonlocal sub-domains. While most LtN coupling methods retain at least some of the above static properties to a certain degree, controlling spurious wave reflections appears to be a much harder task and thus related discussions are excluded from this review.

We point out that the methods described in this review are not tied to a particular discretization. However, the choice of discretization used for local and nonlocal models may affect some of the properties mentioned above. As an example, when the nonlocal discretization does not guarantee asymptotic compatibility, the coupling method will inherit that limitation. Discussions on numerical methods that preserve asymptotic compatibility at the discrete level can be found in [38, 50, 142, 145].

1.3 Outline of the Paper

This review is organized as follows. In Section 2, we introduce the notation, discuss coupling configurations, and describe the mathematical models and recall relevant results, including a description of the nonlocal vector calculus [54, 66]. In Section 3, we provide a description of GDD approaches, i.e., optimization-based methods and the partitioned procedure. Section 4 describes several methods belonging to the group of AtC type coupling approaches, including the Arlequin, morphing, quasi-nonlocal, blending, and splice methods. In Section 5, we present two VH approaches: the energy-based shrinking horizon method and the force-based partial stress method. For each method, we provide a mathematical formulation and describe its properties. We also report relevant numerical results available in the literature with the purpose of illustrating theoretical properties and showing applicability to realistic settings. In Section 6, we draw conclusions and present guidelines for an appropriate choice of LtN coupling methods based on necessities and constraints. The chart in Fig. 1 summarizes the classes of LtN coupling approaches and corresponding methods.

2 Notation, Coupling Configurations, and Mathematical Models

In this section, we introduce the notation and coupling configurations used in this paper (see Section 2.1) and describe the nonlocal models and recall relevant results (see Section 2.2) that will be useful throughout the following sections.

2.1 Nonlocal Variables and Nonlocal Domains

Let $\Omega \subset \mathbb{R}^n$, $n = 1, 2, 3$, be a bounded open domain. We are interested in functions $u : \Omega \to \mathbb{R}$ and $\mathbf{u} : \Omega \to \mathbb{R}^n$, $n = 1, 2, 3$, solutions of nonlocal diffusion and nonlocal mechanics problems, respectively. Specifically, in diffusion, u represents the concentration of a diffusive quantity and, in mechanics, $\mathbf{u}$ represents the displacement in n dimensions.

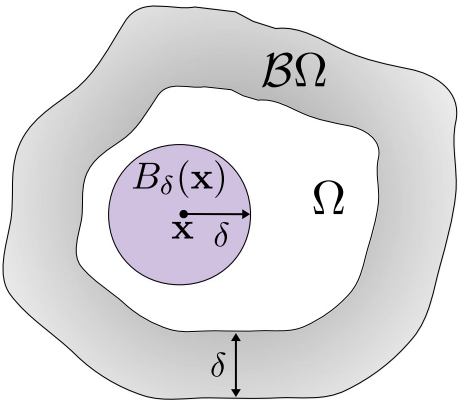

Fig. 2 Domain Ω, nonlocal boundary $\mathcal{B}\Omega$, and nonlocal neighborhood $B_\delta(\mathbf{x})$

In nonlocal settings, every point in a domain interacts with a neighborhood of points. Usually, such neighborhood is an Euclidean ball surrounding points in the domain, i.e.,

$$B_\delta(\mathbf{x}) = \{\mathbf{x}' \in \mathbb{R}^n : \|\mathbf{x}' - \mathbf{x}\| \leqslant \delta\}, \tag{1}$$

where δ is the horizon. This fact has implications on the concept of boundary conditions that are no longer prescribed on $\partial\Omega$, but on a collar of thickness of at least δ surrounding the domain[2] that we refer to as the *nonlocal volumetric boundary domain*, $\mathcal{B}\Omega$, or simply *nonlocal boundary*. This set, by definition, consists of all points outside the domain that interact with points inside the domain. Here, prescription of volume constraints guarantees the well-posedness of the problem [54]. Figure 2 provides a two-dimensional configuration. We denote the union of $\overline{\Omega}$ and $\overline{\mathcal{B}\Omega}$ by $\widehat{\Omega} := \overline{\Omega} \cup \overline{\mathcal{B}\Omega}$, where the overline notation indicates closure in a mathematical sense.

2.1.1 Coupling Configurations

In a general LtN coupling scenario, the domain $\widehat{\Omega}$ is decomposed into a purely local sub-domain (described by the local model), a purely nonlocal sub-domain (described by the nonlocal model), and a transition region connecting those two sub-domains. An illustration is provided in Fig. 3. In the figure, we report both a one-dimensional (left) and a two-dimensional (right) configuration. In the former, the sub-domains are adjacent, whereas, in the latter, the nonlocal sub-domain and transition region are embedded in the local sub-domain.

The way the transition between the purely nonlocal sub-domain and the purely local sub-domain is performed is method-dependent. For instance, in the CH class, we may have either co-existing local and nonlocal models or a hybrid model in the transition region. On the other hand, in the VH class, the transition region could be identified with the region of varying horizon. To provide a better understanding of the differences between the coupling configurations corresponding to the different methods, we illustrate various configurations in Figs. 4, 5, 6, and 7. While any LtN coupling method can be implemented, in

[2] In many nonlocal models, such as bond-based peridynamic models [131], a collar of thickness δ is normally sufficient as nonlocal boundary. However, more general nonlocal models, such as state-based peridynamic models [135], may require a collar of thickness 2δ (see, e.g., [122]).

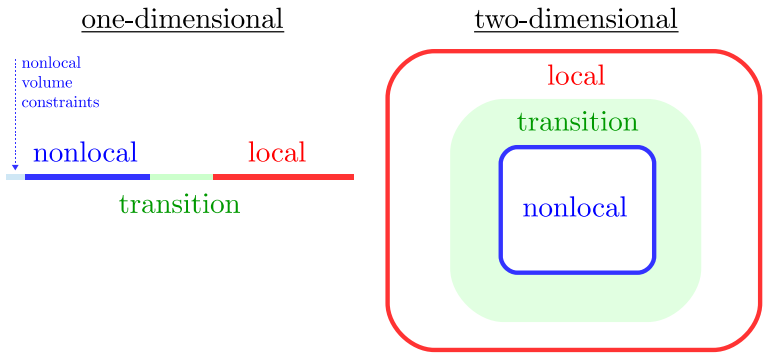

Fig. 3 Illustration of a coupling configuration: the domain is decomposed into a purely nonlocal sub-domain, a transition region, and a purely local sub-domain

general, both on adjacent and embedded configurations, we provide below only the specific configurations used in the following sections.

Domain Decomposition with Overlap We refer to Fig. 4: we report a one-dimensional configuration (top), a two-dimensional configuration with adjacent sub-domains (center), and a two-dimensional configuration with embedded sub-domains (bottom). Here, the transition region is the overlap between the nonlocal and local sub-domains, Ω_{nl} and Ω_l, respectively, where both operators are defined and the solutions co-exist. The domain $\widehat{\Omega}$ is decomposed as $\widehat{\Omega} = \overline{\Omega_l} \cup \widehat{\Omega}_{nl}$, where $\widehat{\Omega}_{nl} = \overline{\Omega}_{nl} \cup \overline{\mathcal{B}\Omega}_{nl}$ is the union of the nonlocal sub-domain and its nonlocal boundary. The overlapping region is defined as $\overline{\Omega}_o := \overline{\Omega_l} \cap \widehat{\Omega}_{nl}$ and includes the local virtual boundary Γ_v and the nonlocal virtual boundary Ω_v. We also introduce the "physical" local and nonlocal boundaries $\Gamma_p = \partial\Omega_l \backslash \Gamma_v$ and $\Omega_p = \mathcal{B}\Omega_{nl} \backslash \Omega_v$, respectively, where we assume that conditions coming from the physics of the problem are provided.

This configuration is used in Sections 3.1, 3.2 (for the overlapping case), and 4.1.

Domain Decomposition without Overlap and with Blending We refer to Fig. 5: we report a one-dimensional configuration (top) and a two-dimensional configuration with embedded sub-domains (bottom). In this decomposition, the nonlocal and local sub-domains do not overlap, but are separated by the transition region, Ω_t. A blending function is used as a partition-of-unity function, which changes in the *blending* region, Ω_b. Due to nonlocal contributions, $\overline{\Omega_t} = \overline{\Omega_b} \cup \overline{\mathcal{B}\Omega_b}$. In the top figure, the domain is decomposed into four disjoint sub-domains: $\widehat{\Omega} = \overline{\Omega_p} \cup \overline{\Omega_{nl}} \cup \overline{\Omega_t} \cup \overline{\Omega_l}$, i.e., the physical nonlocal boundary, the nonlocal sub-domain, the transition region, and the local sub-domain. In the bottom figure, the nonlocal sub-domain is embedded in the local sub-domain and $\widehat{\Omega}$ is decomposed into three disjoint sub-domains: $\widehat{\Omega} = \overline{\Omega_{nl}} \cup \overline{\Omega_t} \cup \overline{\Omega_l}$.

This configuration is used in Sections 4.2 and 4.4.

Domain Decomposition without Overlap and No Blending We refer to Fig. 6: we report a one-dimensional configuration (top) and a two-dimensional configuration with embedded sub-domains (bottom). In the top figure, the domain is decomposed into four disjoint

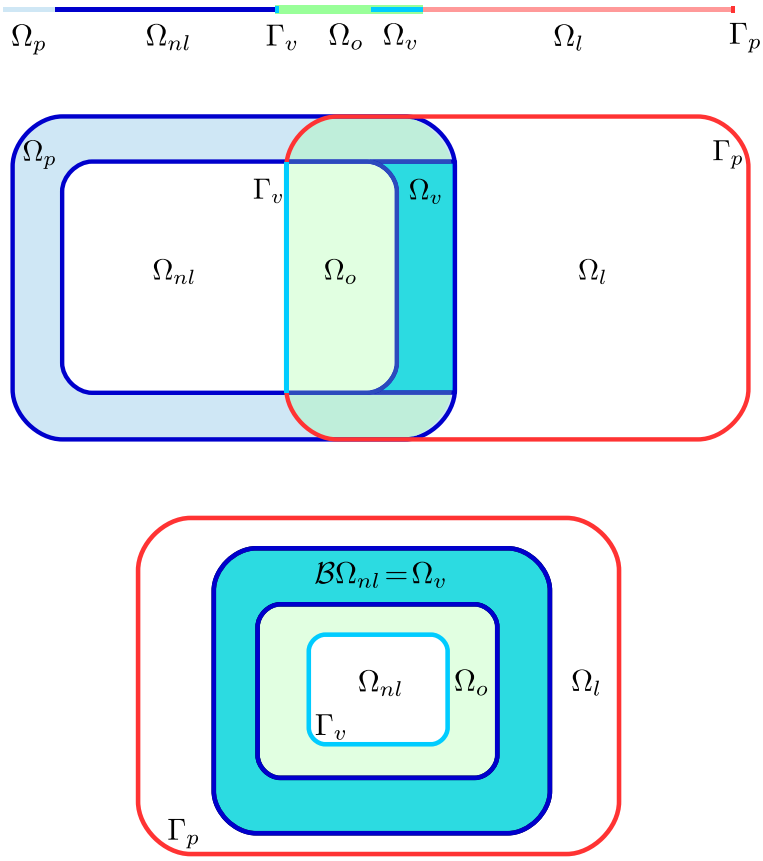

Fig. 4 Coupling configuration in one dimension (top), two dimensions with adjacent sub-domains (center), and two dimensions with embedded sub-domains (bottom). This is a domain decomposition setting with overlap (the green region), where both nonlocal and local solutions co-exist

sub-domains: $\widehat{\Omega} = \overline{\Omega_p} \cup \overline{\Omega_{nl}} \cup \overline{\Omega_t} \cup \overline{\Omega_l}$, i.e., the physical nonlocal boundary, the nonlocal sub-domain, the transition region, and the local sub-domain. In the bottom figure, the nonlocal sub-domain is embedded in the local sub-domain and $\widehat{\Omega}$ is decomposed into three disjoint sub-domains: $\widehat{\Omega} = \overline{\Omega_{nl}} \cup \overline{\Omega_t} \cup \overline{\Omega_l}$.

This configuration is used in Sections 3.2 (for the non-overlapping case), 4.3, 4.5 (with an empty transition region), and 5.2.

Domain Decomposition with Smooth Transition from a Nonlocal to a Local Sub-domain In the case of VH coupling methods, we consider the configurations in Fig. 7 for one-dimensional (top) and two-dimensional (bottom) settings. In these configurations, the domain is decomposed by means of a sharp interface Γ between the nonlocal sub-domain, Ω_{nl}, and the local sub-domain, Ω_l. The extent of the nonlocal interactions decreases as points in the nonlocal sub-domain approach Γ. The same holds true for the nonlocal boundary, that approaches $\partial\widehat{\Omega}_{nl}$ in the area surrounding the interface.

This configuration is used in Section 5.1.

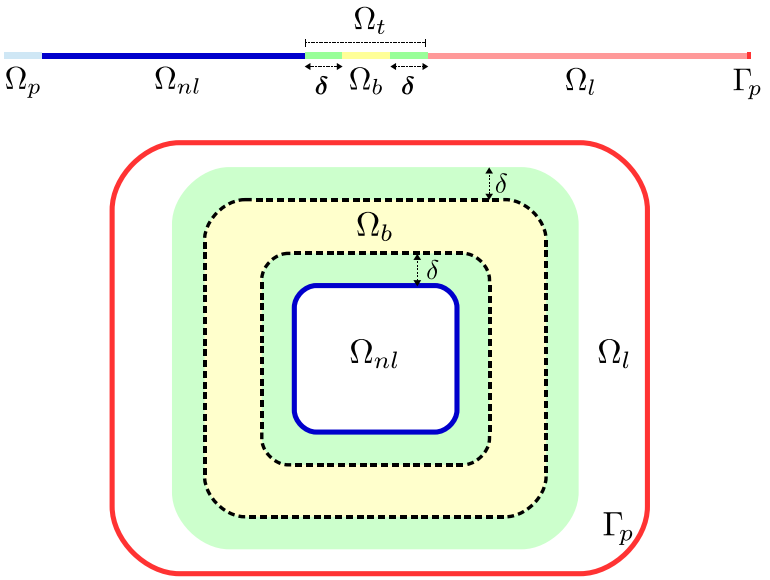

Fig. 5 Coupling configuration in one dimension (top) and two dimensions with embedded sub-domains (bottom) for a setting with a transition region Ω_t (green and yellow) and a blending region Ω_b (yellow). The blending region is part of the transition region and it is δ-apart from the local and nonlocal sub-domains

2.1.2 Illustration of Blending Functions

In various LtN coupling methods, such as Arlequin, morphing, and blending, the idea of a partition of unity is used by means of a blending function, $\beta(\mathbf{x})$, such that

$$\beta(\mathbf{x}) = \begin{cases} 1 & \text{in the purely nonlocal sub-domain,} \\ 0 & \text{in the purely local sub-domain,} \end{cases} \tag{2}$$

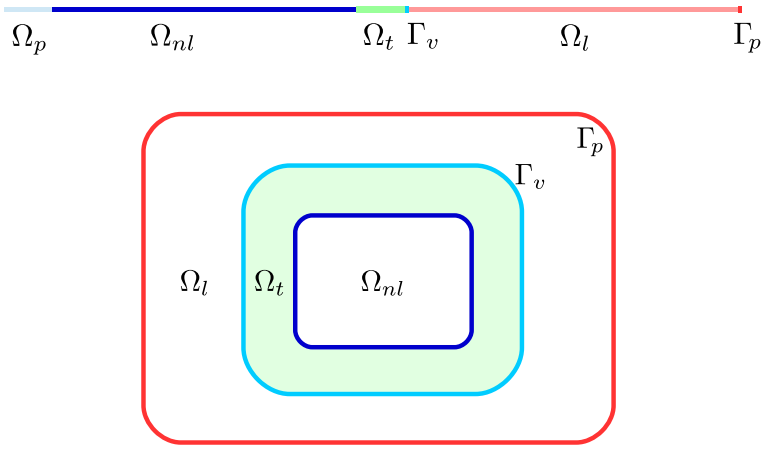

Fig. 6 Coupling configuration in one dimension (top) and two dimensions with embedded sub-domains (bottom) for a setting with a transition region

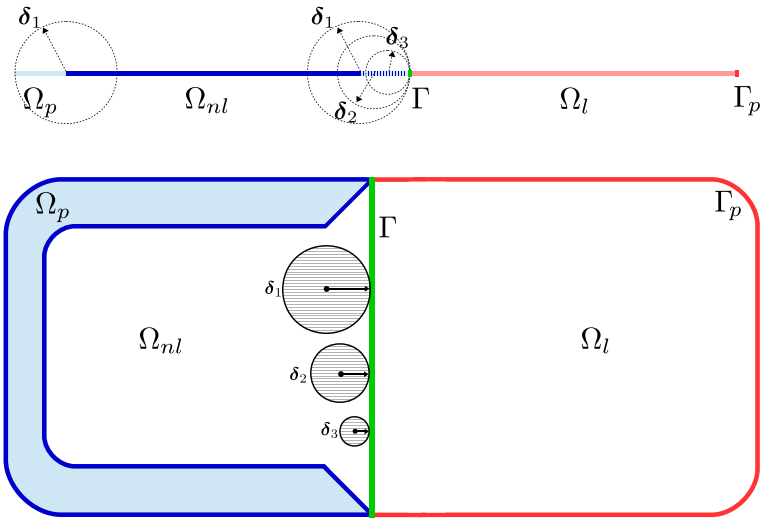

Fig. 7 Coupling configuration in one dimension (top) and two dimensions (bottom) for a variable horizon setting: as $\mathbf{x} \in \Omega_{nl}$ approaches Γ the nonlocal neighborhood linearly shrinks and never crosses the interface

which takes values in the range [0, 1] in the transition region (see Fig. 3). In the Arlequin method, the transition region coincides with the overlapping region, Ω_o (see Fig. 4), and the blending function is chosen as a polynomial, normally constant, linear, or cubic, in that region, as illustrated in one dimension in Fig. 8a. In contrast, in the morphing and blending methods, the polynomial choice of the blending function normally occurs within a sub-region of the transition region referred to as the blending region, Ω_b (see Fig. 5), as illustrated in one dimension in Fig. 8b.

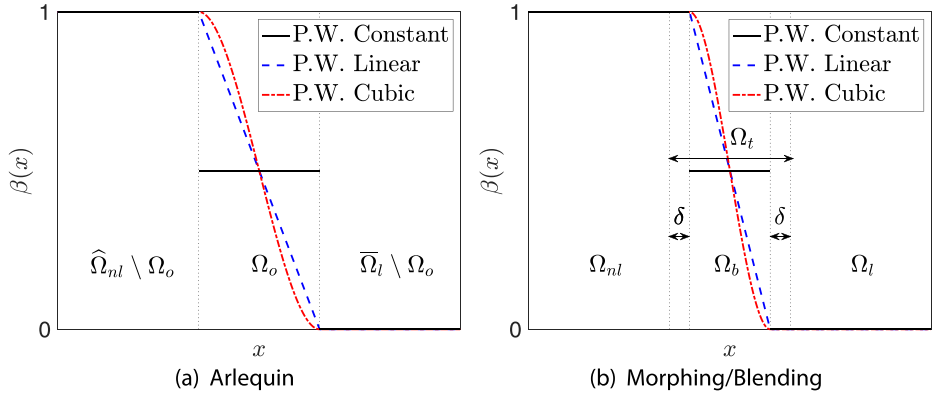

Fig. 8 Illustration of blending functions in one dimension. **a** Domain decomposition with overlap for the Arlequin method. **b** Domain decomposition without overlap and with blending for the morphing and blending methods. Three choices of blending function are shown: piece-wise (P.W.) constant (black solid line), linear (blue dashed line), and cubic (red dashed-dotted line)

2.2 Nonlocal Models

We describe two nonlocal models: nonlocal diffusion and nonlocal mechanics, specifically peridynamics. We recall that in the case of diffusion the unknown is the scalar-valued function u, whereas for mechanics the unknown is the vector-valued function $\mathbf{u}$.

2.2.1 Nonlocal Diffusion

Nonlocal diffusion models have been used in many applications such as describing complex turbulence [10] and nonlocal heat conduction [19] when the classical Fick's first law or standard Brownian motion fail to delineate the underlying phenomena [25, 52, 99, 101].

Given a domain $\Omega \subset \mathbb{R}^n$, the time-dependent nonlocal diffusion equation for a point $\mathbf{x} \in \Omega$ at time $t \geqslant 0$ is

$$\frac{\partial u}{\partial t}(\mathbf{x}, t) = \mathcal{L}^{\mathrm{ND}} u(\mathbf{x}, t) + f(\mathbf{x}, t) = \int_{\mathbb{R}^n} \gamma(\mathbf{x}', \mathbf{x})(u(\mathbf{x}', t) - u(\mathbf{x}, t))\, d\mathbf{x}' + f(\mathbf{x}, t), \quad (3)$$

where $\gamma : \mathbb{R}^n \times \mathbb{R}^n \to \mathbb{R}$ is a symmetric kernel[3] and f is a source. In accordance with the definition of the nonlocal neighborhood, we consider localized kernels of the form

$$\gamma(\mathbf{x}', \mathbf{x}) = \mathcal{X}_{B_\delta}(\mathbf{x}' - \mathbf{x}) k(\mathbf{x}', \mathbf{x}), \quad (4)$$

where

$$\mathcal{X}_B(\mathbf{x}) := \begin{cases} 1 & \mathbf{x} \in B \\ 0 & \text{else} \end{cases} \quad (5)$$

is the characteristic function of a domain B, and we used the notation $B_\delta := B_\delta(\mathbf{0})$ (see (1)). Since, by definition, the nonlocal boundary consists of those points outside of Ω that interact with points inside of Ω, (4) implies that the nonlocal boundary is defined as

$$\mathcal{B}\Omega := \{\mathbf{x}' \in \mathbb{R}^n \setminus \Omega : \|\mathbf{x}' - \mathbf{x}\| \leqslant \delta, \text{ for any } \mathbf{x} \in \Omega\}. \quad (6)$$

As a consequence of (4), for $\mathbf{x} \in \Omega$ the nonlocal operator in (3) reads

$$\mathcal{L}^{\mathrm{ND}} u(\mathbf{x}, t) = \int_{B_\delta(\mathbf{x})} k(\mathbf{x}', \mathbf{x})(u(\mathbf{x}', t) - u(\mathbf{x}, t))\, d\mathbf{x}'. \quad (7)$$

In this work, we mainly focus on static problems, where u depends only on $\mathbf{x}$; we thus omit the time dependence in the remaining of this section. Also, we consider nonlocal diffusion operators that, in the limit of vanishing nonlocality, i.e., as $\delta \to 0$, under suitable regularity assumptions, converge to the classical Laplacian or div-grad operator, Δ or $\nabla \cdot (\nabla)$, respectively. It is possible to show that, when the kernel function $k(\mathbf{x}', \mathbf{x})$ is properly scaled, we have the following property (see, e.g., [40, 139, 156]):

$$\mathcal{L}^{\mathrm{ND}} u(\mathbf{x}) = \Delta u(\mathbf{x}) + \mathcal{O}(\delta^2) \mathrm{D}^{(4)} u(\mathbf{x}), \quad (8)$$

where $\mathrm{D}^{(4)}$ is a combination of the fourth-order derivatives of u.

Remark 1 Property (8) implies that $\mathcal{L}^{\mathrm{ND}}$ and Δ are equivalent for polynomials up to the third order, i.e., $\mathcal{L}^{\mathrm{ND}} p(\mathbf{x}) = \Delta p(\mathbf{x})$, for $p \in \mathbb{P}^3(\mathbb{R}^n)$. Examples of properly scaled kernels, in one dimension, include

$$k(x', x) = \frac{3}{\delta^3} \quad \text{and} \quad k(x', x) = \frac{2}{\delta^2} \frac{1}{|x' - x|}. \quad (9)$$

[3] This discussion could be generalized to non-symmetric [37] or sign-changing [95] kernels.

Note that (8) also implies that the classical Poisson problem is a δ^2-approximation of a nonlocal diffusion problem and, as such, it should be used as the reference local problem in the design of LtN coupling methods. Furthermore, the equivalence property implies that polynomials up to order three are good candidates for patch tests.

We consider nonlocal diffusion problems in the configuration of Fig. 2 and, without loss of generality, we limit our description to the static case. Specifically, given a forcing term $f : \Omega \to \mathbb{R}$ and a volume constraint $g : \mathcal{B}\Omega \to \mathbb{R}$, we solve

$$\begin{cases} -\mathcal{L}^{\mathrm{ND}} u = f & \mathbf{x} \in \Omega, \\ \qquad u = g & \mathbf{x} \in \mathcal{B}\Omega, \end{cases} \tag{10}$$

where the second condition is the nonlocal counterpart of a Dirichlet boundary condition for PDEs. For this reason, we refer to it as Dirichlet volume constraint.[4]

2.2.2 Nonlocal Mechanics

In this paper, the nonlocal mechanics models are provided by the peridynamic theory of solid mechanics. Peridynamics has been applied for material failure and damage simulation (see, e.g., [20, 44]) and seems to provide robust modeling capabilities for analysis of complex crack propagation phenomena, such as branching [23, 70].

Given a domain $\Omega \subset \mathbb{R}^n$, the *state-based* peridynamic equation of motion for a point $\mathbf{x} \in \Omega$ at time $t \geqslant 0$ is [135]

$$\rho(\mathbf{x}) \frac{\partial^2 \mathbf{u}}{\partial t^2}(\mathbf{x}, t) = \mathcal{L}^{\mathrm{PD}} \mathbf{u}(\mathbf{x}, t) + \mathbf{b}(\mathbf{x}, t), \tag{11}$$

where the nonlocal operator in (11) is the peridynamic internal force density,

$$\mathcal{L}^{\mathrm{PD}} \mathbf{u}(\mathbf{x}, t) = \int_{B_\delta(\mathbf{x})} \left\{ \underline{\mathbf{T}}[\mathbf{x}, t]\langle \mathbf{x}' - \mathbf{x} \rangle - \underline{\mathbf{T}}[\mathbf{x}', t]\langle \mathbf{x} - \mathbf{x}' \rangle \right\} d\mathbf{x}', \tag{12}$$

ρ is the mass density, $\underline{\mathbf{T}}$ is the force vector state, and $\mathbf{b}$ is a prescribed body force density. Note that, as for the nonlocal diffusion operator (7), the nonlocal interactions in (12) are restricted to the nonlocal neighborhood. The force vector state $\underline{\mathbf{T}}[\mathbf{x}, t]\langle \boldsymbol{\xi} \rangle$ is an operator defined at a given point $\mathbf{x}$ at time t that maps a peridynamic bond $\boldsymbol{\xi} := \mathbf{x}' - \mathbf{x}$ to force per unit volume squared; this operator contains the constitutive relation characterizing the specific material under consideration. It is sometimes convenient to explicitly indicate the dependence of the force vector state on the deformation. In the case of simple (possibly non-homogeneous) materials, such dependence is expressed as

$$\underline{\mathbf{T}}[\mathbf{x}, t]\langle \boldsymbol{\xi} \rangle = \widehat{\underline{\mathbf{T}}}(\underline{\mathbf{Y}}[\mathbf{x}, t], \mathbf{x})\langle \boldsymbol{\xi} \rangle, \tag{13}$$

where the deformation vector state is defined as

$$\underline{\mathbf{Y}}[\mathbf{x}, t]\langle \boldsymbol{\xi} \rangle := \mathbf{y}(\mathbf{x} + \boldsymbol{\xi}, t) - \mathbf{y}(\mathbf{x}, t) \tag{14}$$

with $\mathbf{y}(\mathbf{x}, t) = \mathbf{x} + \mathbf{u}(\mathbf{x}, t)$ representing the position of point $\mathbf{x}$ in the deformed configuration at time t. Similar to the case of nonlocal diffusion, in this work, we mainly consider static problems, where $\mathbf{u}$ depends only on $\mathbf{x}$; we thus omit the time dependence in the remaining of this section. In addition, it has been shown for elastic materials that, under suitable regularity

[4] Nonlocal Neumann volume constraints are also an option. However, for the sake of clarity and without loss of generality, we do not discuss them.

assumptions, the peridynamic internal force density convergences, in the limit as $\delta \to 0$, to the classical elasticity operator [136], i.e.,

$$\lim_{\delta \to 0} \mathcal{L}^{\mathrm{PD}} \mathbf{u}(\mathbf{x}) = \nabla \cdot \boldsymbol{\nu}^0(\mathbf{x}), \tag{15}$$

where $\boldsymbol{\nu}^0$ is the collapsed peridynamic stress tensor, which is an admissible Piola-Kirchhoff stress tensor defined as [136]

$$\boldsymbol{\nu}^0(\mathbf{x}) := \int_{B_\delta(\mathbf{0})} \widehat{\underline{\mathbf{T}}}(\mathbf{F}(\mathbf{x})\underline{\mathbf{X}}, \mathbf{x})\langle \boldsymbol{\xi} \rangle \otimes \boldsymbol{\xi} d\boldsymbol{\xi}, \tag{16}$$

where $\mathbf{F} := \partial \mathbf{y}/\partial \mathbf{x}$ is the standard deformation gradient tensor and $\underline{\mathbf{X}}\langle \boldsymbol{\xi} \rangle := \boldsymbol{\xi}$ is the reference position vector state.

A special case of state-based peridynamics is when the material response of any bond is independent of other bonds. This is referred to as *bond-based* peridynamics [131] for which the force vector state is given by [135]

$$\underline{\mathbf{T}}[\mathbf{x}]\langle \boldsymbol{\xi} \rangle = \frac{1}{2}\mathbf{f}(\boldsymbol{\eta}, \boldsymbol{\xi}), \tag{17}$$

where $\mathbf{f}$ is the pairwise force function and $\boldsymbol{\eta} := \mathbf{u}(\mathbf{x}+\boldsymbol{\xi}) - \mathbf{u}(\mathbf{x})$ is the relative displacement. In this case,

$$\mathcal{L}^{\mathrm{PD}} \mathbf{u}(\mathbf{x}) = \int_{B_\delta(\mathbf{0})} \mathbf{f}(\boldsymbol{\eta}, \boldsymbol{\xi}) d\boldsymbol{\xi}. \tag{18}$$

We observe that (18) implies that a nonlocal boundary, as in (6), is required to inform points near the domain boundary $\partial\Omega$.

For small deformations, i.e., $\|\boldsymbol{\eta}\| \ll 1$, we can linearize the pairwise force function as[5]

$$\mathbf{f}(\boldsymbol{\eta}, \boldsymbol{\xi}) = \lambda(\boldsymbol{\xi})(\boldsymbol{\xi} \otimes \boldsymbol{\xi})\boldsymbol{\eta}, \tag{19}$$

where λ is a scalar-valued micromodulus function, which in the case of isotropy $\lambda(\boldsymbol{\xi}) = \lambda(\|\boldsymbol{\xi}\|)$. In this case, under a smooth deformation, in the limit as $\delta \to 0$, we have the following property for (18) (similar to (8)) [121]:

$$\mathcal{L}^{\mathrm{PD}} \mathbf{u}(\mathbf{x}) = \mathcal{C}_{ijkl} \frac{\partial^2 u_j}{\partial x_k \partial x_l}(\mathbf{x})\mathbf{e}_i + \mathcal{O}(\delta^2)\mathrm{D}^{(4)}\mathbf{u}(\mathbf{x}), \tag{20}$$

where we used Einstein summation convention for repeated indices and the orthonormal basis $\{\mathbf{e}_1, \mathbf{e}_2, \mathbf{e}_3\}$, and $\mathcal{C}_{ijkl}$ are the components of a fully symmetric fourth-order elasticity tensor, which is related to the micromodulus function by

$$\mathcal{C} = \frac{1}{2}\int_{B_\delta(\mathbf{0})} \lambda(\|\boldsymbol{\xi}\|)\boldsymbol{\xi} \otimes \boldsymbol{\xi} \otimes \boldsymbol{\xi} \otimes \boldsymbol{\xi} d\boldsymbol{\xi}. \tag{21}$$

In the limit as $\delta \to 0$, (20) reduces to the classical linear elasticity operator

$$\mathcal{L}^{\mathrm{CE}} \mathbf{u}(\mathbf{x}) = \begin{cases} \frac{4E}{5}\left[\frac{1}{2}\nabla^2 \mathbf{u}(\mathbf{x}) + \nabla \otimes \nabla \mathbf{u}(\mathbf{x})\right] & \text{in three dimensions,} \\ \frac{3E}{4}\left[\frac{1}{2}\nabla^2 \mathbf{u}(\mathbf{x}) + \nabla \otimes \nabla \mathbf{u}(\mathbf{x})\right] & \text{in two dimensions,} \\ E\frac{\partial^2 u}{\partial x^2}(x) & \text{in one dimension,} \end{cases} \tag{22}$$

[5] We assume a pairwise equilibrated reference configuration, i.e., $\mathbf{f}(\mathbf{0}, \boldsymbol{\xi}) = \mathbf{0}$ for all $\boldsymbol{\xi} \in \mathbb{R}^n$ and neglect terms of order $\mathcal{O}(\|\boldsymbol{\eta}\|^2)$.

where E is Young's modulus. Note that the resulting Poisson's ratio is constrained to $\nu = 1/4$ (in three dimensions) [131] and $\nu = 1/3$ (in two dimensions) [148];[6] this restriction is characteristic of bond-based peridynamics and is removed in state-based peridynamics.

We consider peridynamic problems in the configuration of Fig. 2 and, without loss of generality, we limit our description to the static case. Specifically, given an external body force density $\mathbf{b} : \Omega \to \mathbb{R}^n$ and a volume constraint $\mathbf{g} : \mathcal{B}\Omega \to \mathbb{R}^n$, we solve

$$\begin{cases} -\mathcal{L}^{\mathrm{PD}}\mathbf{u}(\mathbf{x}) = \mathbf{b}(\mathbf{x}) & \mathbf{x} \in \Omega, \\ \mathbf{u}(\mathbf{x}) = \mathbf{g}(\mathbf{x}) & \mathbf{x} \in \mathcal{B}\Omega, \end{cases} \tag{23}$$

where the second condition is, as in the nonlocal diffusion case, a Dirichlet volume constraint.

2.2.3 Nonlocal Vector Calculus

In this section, we reformulate nonlocal diffusion and peridynamic operators in terms of the *nonlocal vector calculus* developed in [66]. This theory is the nonlocal counterpart of the classical calculus for differential operators and, by providing a variational setting, allows one to analyze nonlocal problems in a very similar way as for PDEs. Such calculus is necessary to analyze several LtN coupling methods described in this review; as such, we report relevant results and refer the reader to [53, 54, 66, 96] for more details.

Following the notations in [54], the *nonlocal divergence operator* $\mathcal{D}$ acting on a two-point function $\boldsymbol{\nu}(\mathbf{x}, \mathbf{x}') : \mathbb{R}^n \times \mathbb{R}^n \to \mathbb{R}^n$ is defined as

$$(\mathcal{D}\boldsymbol{\nu})(\mathbf{x}) := \int_{\mathbb{R}^n} (\boldsymbol{\nu}(\mathbf{x}, \mathbf{x}') + \boldsymbol{\nu}(\mathbf{x}', \mathbf{x})) \cdot \boldsymbol{\alpha}(\mathbf{x}, \mathbf{x}') d\mathbf{x}' ,$$

where $\boldsymbol{\alpha}(\mathbf{x}, \mathbf{x}')$ is anti-symmetric, i.e., $\boldsymbol{\alpha}(\mathbf{x}, \mathbf{x}') = -\boldsymbol{\alpha}(\mathbf{x}', \mathbf{x})$. Without loss of generality, we assume

$$\boldsymbol{\alpha}(\mathbf{x}, \mathbf{x}') = \frac{\mathbf{x}' - \mathbf{x}}{\|\mathbf{x}' - \mathbf{x}\|}. \tag{24}$$

The adjoint operator of $\mathcal{D}$, $\mathcal{D}^*$, acting on a one-point function $u(\mathbf{x}) : \mathbb{R}^n \to \mathbb{R}$ is defined by

$$(\mathcal{D}^* u)(\mathbf{x}, \mathbf{x}') := -(u(\mathbf{x}') - u(\mathbf{x}))\boldsymbol{\alpha}(\mathbf{x}, \mathbf{x}') .$$

Using the notations of nonlocal divergence and gradient operators, the nonlocal diffusion operator $\mathcal{L}^{\mathrm{ND}}$ in (3) is then written as

$$\mathcal{L}^{\mathrm{ND}} u(\mathbf{x}) = -\frac{1}{2}\mathcal{D}(\gamma \mathcal{D}^* u)(\mathbf{x}) ,$$

where $\gamma = \gamma(\mathbf{x}', \mathbf{x})$ is the kernel defined in Section 2.2.1. We next define the energy functional associated with the problem (10):

$$\begin{aligned} E_\delta^{\mathrm{ND}}(u, f, g) := \frac{1}{4} \int_{\widehat{\Omega}} \int_{\widehat{\Omega}} \gamma(\mathbf{x}', \mathbf{x})((\mathcal{D}^* u)(\mathbf{x}', \mathbf{x}))^2 d\mathbf{x}' d\mathbf{x} \\ - \int_\Omega f(\mathbf{x}) u(\mathbf{x}) d\mathbf{x} - \int_{\mathcal{B}\Omega} g(\mathbf{x}) u(\mathbf{x}) d\mathbf{x}. \end{aligned}$$

[6] We point out that in (22) the operator in two dimensions corresponds to a pure two-dimensional model, which coincides with a *plane stress* formulation [147]. Peridynamic isotropic plane stress models are restricted by a Poisson's ratio of $\nu = 1/3$, whereas peridynamic isotropic *plane strain* models are restricted by a Poisson's ratio of $\nu = 1/4$ [59, 148].

The corresponding energy norm, energy space, and constrained energy space are then given, respectively, by

$$\begin{aligned} \|u\|_{\mathrm{ND}} &= (E_\delta^{\mathrm{ND}}(u,0,0))^{1/2}, \\ \mathcal{S}^{\mathrm{ND}}(\widehat{\Omega}) &= \{u \in L^2(\widehat{\Omega}) : \|u\|_{\mathrm{ND}} < \infty\}, \\ \mathcal{S}_c^{\mathrm{ND}}(\widehat{\Omega}) &= \{u \in \mathcal{S}^{\mathrm{ND}}(\widehat{\Omega}) : u|_{\mathcal{B}\Omega} = 0\}. \end{aligned}$$

Given the two-point function $\boldsymbol{\Psi} : \mathbb{R}^n \times \mathbb{R}^n \to \mathbb{R}^{n\times n}$ and the one-point function $\mathbf{u} : \mathbb{R}^n \to \mathbb{R}^n$, we can similarly define the nonlocal divergence operator $\mathcal{D}$ and its adjoint $\mathcal{D}^*$ by

$$\begin{aligned} (\mathcal{D}\boldsymbol{\Psi})(\mathbf{x}) &:= \int_{\mathbb{R}^n} (\boldsymbol{\Psi}(\mathbf{x}',\mathbf{x}) + \boldsymbol{\Psi}(\mathbf{x},\mathbf{x}')) \cdot \boldsymbol{\alpha}(\mathbf{x},\mathbf{x}') d\mathbf{x}', \\ (\mathcal{D}^*\mathbf{u})(\mathbf{x},\mathbf{x}') &:= -(\mathbf{u}(\mathbf{x}') - \mathbf{u}(\mathbf{x})) \otimes \boldsymbol{\alpha}(\mathbf{x},\mathbf{x}'), \end{aligned}$$

where $\boldsymbol{\alpha}$ is given by (24). The linear bond-based peridynamic operator $\mathcal{L}^{\mathrm{PD}}$ in (18) with (19) is then written as

$$\mathcal{L}^{\mathrm{PD}}(\mathbf{x}) = -\frac{1}{2}\mathcal{D}(\gamma(\mathcal{D}^*\mathbf{u})^T)(\mathbf{x}),$$

where $\gamma = \gamma(\mathbf{x}',\mathbf{x}) := \mathcal{X}_{B_\delta}(\mathbf{x}'-\mathbf{x})\lambda(\|\mathbf{x}'-\mathbf{x}\|)\|\mathbf{x}'-\mathbf{x}\|^2$. We can also define the energy functional for problem (23):

$$\begin{aligned} E_\delta^{\mathrm{PD}}(\mathbf{u},\mathbf{b},\mathbf{g}) := \frac{1}{4}\int_{\widehat{\Omega}}\int_{\widehat{\Omega}} \gamma(\mathbf{x}',\mathbf{x})(\mathrm{Tr}(\mathcal{D}^*\mathbf{u})(\mathbf{x},\mathbf{x}'))^2 d\mathbf{x}' d\mathbf{x} \\ - \int_\Omega \mathbf{b}(\mathbf{x})\mathbf{u}(\mathbf{x}) d\mathbf{x} - \int_{\mathcal{B}\Omega} \mathbf{g}(\mathbf{x})\mathbf{u}(\mathbf{x}) d\mathbf{x}, \end{aligned}$$

where $\mathrm{Tr}(\mathcal{D}^*\mathbf{u})$ is the trace of $\mathcal{D}^*\mathbf{u}$. The corresponding energy norm, energy space, and constrained energy space are given, respectively, by

$$\begin{aligned} \|\mathbf{u}\|_{\mathrm{PD}} &= (E_\delta^{\mathrm{PD}}(\mathbf{u},\mathbf{0},\mathbf{0}))^{1/2}, \\ \mathcal{S}^{\mathrm{PD}}(\widehat{\Omega}) &= \{\mathbf{u} \in L^2(\widehat{\Omega},\mathbb{R}^n) : \|\mathbf{u}\|_{\mathrm{PD}} < \infty\}, \\ \mathcal{S}_c^{\mathrm{PD}}(\widehat{\Omega}) &= \{\mathbf{u} \in \mathcal{S}^{\mathrm{PD}}(\widehat{\Omega}) : \mathbf{u}|_{\mathcal{B}\Omega} = \mathbf{0}\}. \end{aligned}$$

Note that $L^2(\widehat{\Omega}) = L^2(\widehat{\Omega},\mathbb{R})$ is the space of $\mathbb{R}$-valued square-integrable functions on Ω under our notation.

The nonlocal energy spaces $\mathcal{S}^{\mathrm{ND}}(\widehat{\Omega})$ and $\mathcal{S}^{\mathrm{PD}}(\widehat{\Omega})$ defined above are Hilbert spaces, as shown in [95, 96]. Moreover, the nonlocal diffusion problem (10) and the nonlocal mechanics problem (23) are well-posed as a result of nonlocal Poincaré type inequalities. Here we state the inequalities without proof, and more details can be found in [52, 95, 96].

Lemma 1 (**Nonlocal Poincaré inequalities**) *There exists a positive constant C such that the following Poincaré type inequalities hold:*

$$\begin{aligned} \|u\|_{L^2(\widehat{\Omega})} &\leqslant C\|u\|_{\mathrm{ND}}, \quad \forall u \in \mathcal{S}_c^{\mathrm{ND}}(\widehat{\Omega}), \\ \|\mathbf{u}\|_{L^2(\widehat{\Omega},\mathbb{R}^n)} &\leqslant C\|\mathbf{u}\|_{\mathrm{PD}}, \quad \forall \mathbf{u} \in \mathcal{S}_c^{\mathrm{PD}}(\widehat{\Omega}). \end{aligned}$$

We only presented the reformulation of nonlocal diffusion and bond-based peridynamics in the above. However, state-based peridynamics can also be reformulated using the nonlocal vector calculus and details can be found in [50, 53, 97].

3 Generalized Domain Decomposition Methods

3.1 Optimization-Based Methods

In optimization-based methods (OBMs) the coupling of local and nonlocal models is effected by couching the LtN coupling into an optimization problem. This approach is inspired by GDD methods for PDEs [45, 49, 55, 60, 67–69] and it has also been applied to AtC coupling in [105, 106]. A main feature of OBMs is that numerical solutions only require the implementation of the optimization strategy as the local and nonlocal solvers can be used as black boxes. For this reason, OB couplings (OBCs) are considered *non-intrusive* as opposed to other methods whose implementation requires modification of the basic governing equations in the transition region between local and nonlocal sub-domains.

3.1.1 Mathematical Formulation

We provide a very general formulation of an OBM. Let $\mathcal{L}^{\mathrm{NL}}$ be a nonlocal operator that accurately describes the system in a bounded domain Ω and let $\mathcal{L}^{\mathrm{L}}$ be a corresponding local operator that describes the system well enough where nonlocal effects are negligible. OBMs tackle the LtN coupling by solving a minimization problem where the difference between the local and nonlocal solutions is minimized in the overlap between local and nonlocal sub-domains, tuning their values on the virtual boundaries induced by the domain decomposition (see Fig. 4). Here, we state the LtN OBC in a very general form for vector functions:

$$\min_{\mathbf{u}^{nl},\mathbf{u}^{l},\boldsymbol{v}^{nl},\boldsymbol{v}^{l}} \frac{1}{2}\|\mathbf{u}^{nl}-\mathbf{u}^{l}\|^2_{*,\Omega_o} \quad \text{such that}$$

$$\begin{cases} -\mathcal{L}^{\mathrm{NL}}\mathbf{u}^{nl}=\mathbf{b} & \mathbf{x}\in\Omega_{nl} \\ \mathbf{u}^{nl}=\mathbf{g} & \mathbf{x}\in\Omega_p \\ \mathbf{u}^{nl}=\boldsymbol{v}^{nl} & \mathbf{x}\in\Omega_v \end{cases} \quad \text{and} \quad \begin{cases} -\mathcal{L}^{\mathrm{L}}\mathbf{u}^{l}=\mathbf{b} & \mathbf{x}\in\Omega_{l} \\ \mathbf{u}^{l}=\mathbf{g} & \mathbf{x}\in\Gamma_p \\ \mathbf{u}^{l}=\boldsymbol{v}^{l} & \mathbf{x}\in\Gamma_v \end{cases}, \tag{25}$$

where $\mathbf{b}$ is a forcing term over $\Omega_{nl}\cup\Omega_l$, $\mathbf{g}$ is a boundary data over Ω_p and Γ_p, $\|\cdot\|_{*,\Omega_o}$ is a suitable norm in the overlapping region Ω_o, and $(\boldsymbol{v}^{nl},\boldsymbol{v}^{l})\in\mathcal{C}$ (an appropriate control space) are the control variables. The goal of OBC is to find optimal values for the virtual controls $\boldsymbol{v}^{nl}$ and $\boldsymbol{v}^{l}$ such that the nonlocal and local solutions, $\mathbf{u}^{nl}$ and $\mathbf{u}^{l}$, respectively, are as close as possible in the overlapping region, while still satisfying their corresponding governing equations. We denote the *optimal* controls and corresponding nonlocal and local solutions by $(\boldsymbol{v}^{nl*},\boldsymbol{v}^{l*})$ and $(\mathbf{u}^{nl*},\mathbf{u}^{l*})$, respectively. The global coupled solution is then defined as

$$\mathbf{u}^{*}(\mathbf{x})=\mathbf{u}^{nl*}(\mathbf{x})\,\mathcal{X}_{\Omega_{nl}}(\mathbf{x})+\mathbf{u}^{l*}(\mathbf{x})\,\mathcal{X}_{\Omega_l\setminus\Omega_o}(\mathbf{x}) \qquad \text{for all } \mathbf{x}\in\Omega, \tag{26}$$

where $\mathcal{X}_{\Omega_{nl}}(\cdot)$ and $\mathcal{X}_{\Omega_l}(\cdot)$ are the characteristic functions of Ω_{nl} and Ω_l, respectively (see (5)).

Applications of this technique to nonlocal diffusion can be found in [34, 35] in one dimension and in [39] in three dimensions, whereas applications to nonlocal mechanics can be found in [20].

We now present a more rigorous formulation of OBC for a nonlocal diffusion problem, following [35]. In this case, the unknowns are the scalar-valued functions $u^{nl}\in\mathcal{S}_c^{\mathrm{ND}}(\widehat{\Omega}_{nl})$

and $u^l \in H^1_{\Gamma_p}(\Omega_l)$[7] such that

$$\begin{cases} -\mathcal{L}^{\mathrm{ND}} u^{nl} = f & \mathbf{x} \in \Omega_{nl} \\ u^{nl} = 0 & \mathbf{x} \in \Omega_p \\ u^{nl} = v^{nl} & \mathbf{x} \in \Omega_v \end{cases} \quad \text{and} \quad \begin{cases} -\Delta u^l = f & \mathbf{x} \in \Omega_l \\ u^l = 0 & \mathbf{x} \in \Gamma_p \\ u^l = v^l & \mathbf{x} \in \Gamma_v \end{cases}, \tag{27}$$

where $\mathcal{L}^{\mathrm{ND}}$ is the nonlocal diffusion operator introduced in Section 2.2.1 and $(v^{nl}, v^l) \in \mathcal{C} := \widetilde{\mathcal{S}}_c^{\mathrm{ND}} \times H^{\frac{1}{2}}(\Gamma_v)$, where $\widetilde{\mathcal{S}}_c^{\mathrm{ND}} = \{v|_{\Omega_v} : v \in \mathcal{S}_c^{\mathrm{ND}}(\widehat{\Omega}_{nl})\}$ and $v|_{\Omega_v}$ denotes a restriction of v to Ω_v, are the undetermined Dirichlet volume constraint for the nonlocal problem and the undetermined Dirichlet boundary condition for the PDE. Thus, the OBC can be formulated as the following constrained optimization problem:

$$\min_{u^{nl}, u^l, v^{nl}, v^l} \frac{1}{2} \|u^{nl} - u^l\|^2_{L^2(\Omega_o)} \quad \text{subjected to Eq. (27).} \tag{28}$$

Given the optimal controls (v^{nl*}, v^{l*}), the global coupled solution is defined as in (26).

Properties OBC approaches such as (28) have several desirable properties:

- Provided that the nonlocal and local problems are well-posed (see Section 2.2.3), the optimal control problem is well-posed, i.e., (28) has a unique solution. In particular, it is possible to show that the Euler-Lagrange equations associated with the reduced functional $\mathcal{J}(v^{nl}, v^l) = \frac{1}{2}\|u^{nl}(v^{nl}) - u^l(v^l)\|^2_{L^2(\Omega_o)}$ define a coercive variational form in the control space $\mathcal{C}$ [35, 39], where the notations $u^{nl}(v^{nl})$ and $u^l(v^l)$ denote the solutions u^{nl} and u^l given the virtual controls v^{nl} and v^l, respectively.
- When $\mathcal{L}^{\mathrm{ND}}$ is properly scaled (see Remark 1), the method passes the linear, quadratic, and cubic patch tests. Furthermore, [35] shows that as $\delta \to 0$ the coupled solution approaches the solution of a global local problem, i.e., the method is asymptotically compatible. However, this result can only be achieved as long as the overlapping region Ω_o is "large enough," as convergence estimates depend on $|\Omega_o|^{-1}$, where $|\Omega_o|$ denotes the size of Ω_o.
- The numerical solution of nonlocal and local problems is completely uncoupled. As a consequence, nonlocal and local governing equations can be discretized on separate computational sub-domains with different discretization methods (e.g., meshfree method for the nonlocal equation and the FEM for the local equation). This implies that available software for the solution of each problem can be used as a black box.
- The mathematical formulation presented in this section can be easily extended to the peridynamic model presented in Section 2.2.2 by simply substituting $\mathcal{L}^{\mathrm{NL}}$ with $\mathcal{L}^{\mathrm{PD}}$, either in the state-based or bond-based forms, and $\mathcal{L}^{\mathrm{L}}$ with the corresponding classical elasticity operator (e.g., $\mathcal{L}^{\mathrm{CE}}$ in (22) for bond-based peridynamics), as demonstrated in Section 3.1.2.
- The optimization does not affect the rate of convergence of the discretization method used for the governing equations (e.g., a piece-wise linear FEM discretization preserves second-order convergence of the solution in the L^2-norm).

The Time-Dependent Problem The extension of this method to time-dependent problems is straightforward. However, due to the high computational cost of the optimization problem, it still has limited applicability. Such extension consists in performing the optimization at every time step of the time integration. Specifically, at every time step the objective

[7] We denote by $H^1_{\Gamma_p}(\Omega_l)$ the space of functions in $H^1(\Omega_l)$ that vanish on Γ_p.

functional is the same as in (25), but the constraints are the semi-discrete (in time) nonlocal and local problems. An even more expensive option is to formulate the time-dependent coupling as a continuous global (in space and time) optimization problem, where the objective functional is the norm of the misfits over the whole space-time domain and the constraints are the time-dependent nonlocal and local problems. None of these approaches has been rigorously analyzed nor implemented.

3.1.2 Applications and Results

As anticipated in the previous section, the abstract formulation in (25) can be easily extended to state-based peridynamics. Here, we report results for the linearized version (see [133]) of the linear peridynamic solid model introduced in [135]. This is an isotropic state-based peridynamic model that converges, in the limit as $\delta \to 0$ and under suitable regularity assumptions, to classical linear elasticity without the Poisson's ratio restriction discussed in Section 2.2.2. We report linear and quadratic patch tests for a stainless steel bar as obtained in [20] (where all the specifics are listed). In both tests, the nonlocal problem is discretized using a meshfree method [134] (see also [85]) and the local problem is discretized using piece-wise linear FEM. The computational domain is reproduced in Fig. 9. On the left, the nonlocal problem is discretized with a meshfree method; on the right, the local problem is discretized with FEM. Results are reproduced in Fig. 10, where displacement solutions in the horizontal direction are reported along a horizontal line passing through the center of the bar. The patch test results are in good agreement with the expected linear and quadratic solutions for both the fully nonlocal and local problems.

Further results in [20] for stainless steel bars with cracks demonstrate the ability of OBC to capture cracks in nonlocal regions as well as the ease of dealing with boundary conditions that can be applied to local regions circumventing the non-trivial task of prescribing nonlocal boundary conditions.

3.2 Partitioned Procedure

In this section we introduce another GDD type method, known as partitioned procedure, which can be applied to heterogeneous domains such as those characterized by multi-scale and multi-physics dynamics. In the partitioned procedure, the coupled problem is solved based on iterative solutions of sub-problems. The sub-problems are coupled through transmission conditions on interfaces, which enforce the continuity of solutions and

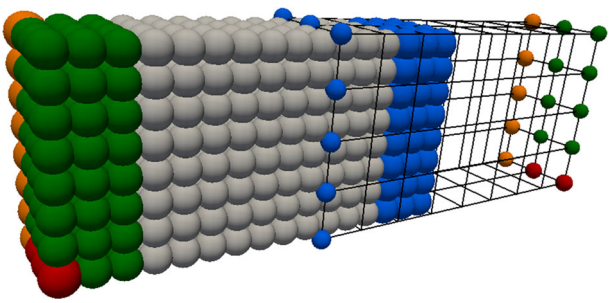

Fig. 9 Computational domain for linear and quadratic patch tests for the optimization-based method. On the right, a meshfree discretization; on the left, a FEM discretization. Blue nodes indicate the control variables degrees of freedom

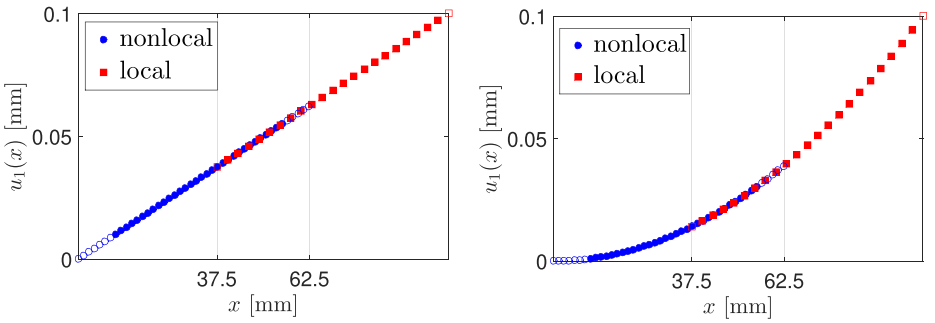

(a) Linear Patch Test (b) Quadratic Patch Test

Fig. 10 Patch tests for the optimization-based method: linear (left) and quadratic (right). The figures show displacements along the horizontal line passing through the center of the bar presented in Fig. 9; u_1 stands for the component of the displacement in the x-direction. Nodes in the nonlocal sub-domain are represented by blue filled circles, whereas nodes in the (physical and virtual) nonlocal boundaries are represented by empty blue circles. Nodes in the local sub-domain are represented by red filled squares, whereas nodes on the (physical and virtual) local boundaries are represented by empty red squares

the energy balance of the whole system. One of the main features of this approach is software modularity. In fact, since each sub-problem is solved separately, possibly with different solvers, the partitioned procedure allows for the reuse of existing codes/discretization methods. Moreover, because only transmission conditions on the coupling interfaces are needed and provided for each solver, the partitioned procedure is also generally non-intrusive, similar to OBMs.

While the partitioned procedure can be applied to static and quasi-static problems, it is more commonly used for dynamic problems. Therefore, we describe the partitioned formulation for dynamic LtN coupling problems. The partitioned procedure can be broadly classified as either explicit or implicit (in the literature these two approaches are sometimes referred to as loosely coupled strategy and strongly coupled strategy, respectively). In explicit coupling strategies, the solution of each sub-problem and the exchange of interface data are performed only once (or a small number of times) per time step. For reasons pointed out below, this causes an information mismatch on the interface. As a consequence, the coupled system does not satisfy exactly the coupling transmission conditions and the energy exchanged between sub-problems is not perfectly balanced. In contrast, in implicit coupling strategies, each sub-problem is solved iteratively until convergence is reached. Thus, transmission conditions are always satisfied and the energy of the system is balanced. This generally allows one to achieve numerical stability, even for highly nonlinear coupled systems.

The partitioned procedure formulation for LtN coupling is introduced in [157] for nonlocal diffusion problems and in [158] for nonlocal mechanics problems. In both works, the authors use Robin transmission conditions since, compared with Dirichlet and Neumann transmission conditions, are more flexible and often more robust.

3.2.1 Mathematical Formulation

To introduce the partitioned procedure formulation for LtN coupling with Robin transmission conditions, we consider a general time-dependent LtN coupling problem. At time step k and sub-iteration j, we solve for $\mathbf{u}^{nl}_{k,j}$ and $\mathbf{u}^{l}_{k,j}$ using the solutions at the previous time

step, $\mathbf{u}^{nl}_{k-1}$ and $\mathbf{u}^{l}_{k-1}$, and the solutions at the previous sub-iteration, $\mathbf{u}^{nl}_{k,j-1}$ and $\mathbf{u}^{l}_{k,j-1}$. Note that $\mathbf{u}^{l}_{k,0}$ and $\mathbf{u}^{nl}_{k,0}$ are taken as the solutions from the previous time step, $\mathbf{u}^{l}_{k-1}$ and $\mathbf{u}^{nl}_{k-1}$, respectively. We first describe the partitioned procedure for the overlapping case, i.e., with a configuration corresponding to Fig. 4:

$$
\begin{cases}
D_t \mathbf{u}^{nl}_{k,j} - \mathcal{L}^{\mathrm{NL}} \mathbf{u}^{nl}_{k,j} = \mathbf{s}_k & \mathbf{x} \in \Omega_{nl}, \\
\mathbf{u}^{nl}_{k,j} = \mathbf{g}_k & \mathbf{x} \in \Omega_p, \\
R_1 \mathbf{u}^{nl}_{k,j} + T^{\mathrm{NL}}(\mathbf{u}^{nl}_{k,j}) = R_1 \mathbf{u}^{l}_{k,j-1} + T^{\mathrm{L}}(\mathbf{u}^{l}_{k,j-1}) & \mathbf{x} \in \Omega_v,
\end{cases}
\qquad
\begin{cases}
D_t \mathbf{u}^{l}_{k,j} - \mathcal{L}^{\mathrm{L}} \mathbf{u}^{l}_{k,j} = \mathbf{s}_k & \mathbf{x} \in \Omega_l, \\
\mathbf{u}^{l}_{k,j} = \mathbf{g}_k & \mathbf{x} \in \Gamma_p, \\
R_2 \mathbf{u}^{l}_{k,j} + T^{\mathrm{L}}(\mathbf{u}^{l}_{k,j}) = R_2 \mathbf{u}^{nl}_{k,j} + T^{\mathrm{NL}}(\mathbf{u}^{nl}_{k,j}) & \mathbf{x} \in \Gamma_v,
\end{cases}
\tag{29}
$$

where $\mathbf{s}$ is a forcing term over $\Omega_{nl} \cup \Omega_l$ and $\mathbf{g}$ is a boundary data over Ω_p and Γ_p. For diffusion problems, $\mathbf{u}$ is a scalar-valued function, $\mathcal{L}^{\mathrm{NL}} = \mathcal{L}^{\mathrm{ND}}$, $\mathcal{L}^{\mathrm{L}} = \Delta$, and $\mathbf{s} = f$ (see Section 2.2.1). For mechanics problems, $\mathbf{u}$ is a vector-valued function, $\mathcal{L}^{\mathrm{NL}}\mathbf{u}(\mathbf{x}, t) = \frac{1}{\rho(\mathbf{x})}\mathcal{L}^{\mathrm{PD}}\mathbf{u}(\mathbf{x}, t)$, $\mathcal{L}^{\mathrm{L}}\mathbf{u}(\mathbf{x}, t) = \frac{1}{\rho(\mathbf{x})}\nabla \cdot \boldsymbol{\nu}^0(\mathbf{x}, t)$, and $\mathbf{s}(\mathbf{x}, t) = \frac{\mathbf{b}(\mathbf{x},t)}{\rho(\mathbf{x})}$ (see Section 2.2.2). T^{L} is a flux operator in diffusion problems or a normal stress operator in mechanics problems, and T^{NL} is a corresponding nonlocal operator to be defined. D_t is the appropriate finite-difference operator that approximates a first-order time derivative (in diffusion problems) or a second-order time derivative (in mechanics problems) of $\mathbf{u}$. R_1 and R_2 are constant Robin coefficients. Note that when $R_i = 0, i = 1, 2$, the Robin transmission condition is equivalent to a Neumann-type transmission condition, whereas when $R_i \to \infty, i = 1, 2$, the Dirichlet transmission condition is obtained. In the explicit partitioned procedure, the solutions are updated as $\mathbf{u}^{nl}_{k} = \mathbf{u}^{nl}_{k,j}$ and $\mathbf{u}^{l}_{k} = \mathbf{u}^{l}_{k,j}$ after one or a few sub-iterations. Note that in the explicit partitioned procedure, the Robin transmission condition in the nonlocal sub-problem becomes $R_1\mathbf{u}^{nl}_{k} + T^{\mathrm{NL}}(\mathbf{u}^{nl}_{k}) = R_1\mathbf{u}^{l}_{k-1} + T^{\mathrm{L}}(\mathbf{u}^{l}_{k-1})$, so the transmission condition $R_1\mathbf{u}^{nl} + T^{\mathrm{NL}}(\mathbf{u}^{nl}) = R_1\mathbf{u}^{l} + T^{\mathrm{L}}(\mathbf{u}^{l})$ is not exactly satisfied, and therefore the energy of the system is not balanced. In the implicit partitioned procedure, the sub-iterations stop only when a prescribed stopping criterion is reached, and as a consequence the energy exchanged on the interface is balanced. To apply Robin transmission conditions in LtN coupling problems, one of the challenges is to provide a well-defined nonlocal operator T^{NL}. In the overlapping case, both local and nonlocal solutions exist in Ω_o. In [158], the authors proposed to employ the local operator $T^{\mathrm{L}}(\mathbf{u}^{nl})$ as an approximation of the nonlocal operator $T^{\mathrm{NL}}(\mathbf{u}^{nl})$.

In [157], the authors considered a coupling configuration for the non-overlapping case as in Fig. 6; here, the transition region, Ω_t, corresponds to the nonlocal Neumann boundary and the sharp interface, Γ_v, is where local and nonlocal models interact. For the local sub-problem, a Dirichlet transmission condition $u^{l}_{k,j} = u^{nl}_{k,j}$ is employed on Γ_v. For the nonlocal sub-problem, instead of explicitly defining the nonlocal Neumann-type operator T^{NL}, the authors developed a nonlocal formulation which converts the local flux to a correction term in the nonlocal model and provides an estimate for the nonlocal interactions across Γ_v. For $\mathbf{x} \in \Omega_t$, where Ω_t is a collar of thickness δ adjacent to the LtN coupling interface (see Fig. 6), a modified nonlocal formulation is employed:

$$
\begin{aligned}
&Q_\delta(\mathbf{x}) D_t \mathbf{u}^{nl}_{k,j}(\mathbf{x}, t) - \mathcal{L}^{\mathrm{NL}}_{N\delta}\mathbf{u}^{nl}_{k,j}(\mathbf{x}, t) + R_1 V_\delta(\mathbf{x})\mathbf{u}^{nl}_{k,j}(P(\mathbf{x}), t) \\
&= Q_\delta(\mathbf{x})\mathbf{s}_k(\mathbf{x}, t) + V_\delta(\mathbf{x})T^{\mathrm{L}}(\mathbf{u}^{l}_{k,j-1}(P(\mathbf{x}), t)) + R_1 V_\delta(\mathbf{x})\mathbf{u}^{l}_{k,j-1}(P(\mathbf{x}), t),
\end{aligned}
$$

where Q_δ and V_δ are functions of $\mathbf{x}$, P is the projection operator onto Γ_v, and $\mathcal{L}_{N\delta}^{\mathrm{NL}}$ is a modified nonlocal operator as proposed in [157]. This formulation provides a generalization of the classical local Robin transmission condition, such that the nonlocal problem converges to the corresponding local problem with local Robin transmission condition, as $\delta \to 0$, under suitable regularity assumptions.

Properties To achieve a stable and/or fast convergent LtN coupling algorithm, one needs to choose optimal Robin coefficients, R_1 and R_2; see next section. With proper Robin coefficients, the partitioned procedure has several properties:

- The partitioned procedure is not tied to any particular discretization. Actually, it provides a flexible coupling framework which enables software modularity: different discretization methods, including different spatial and time resolutions, can be employed for the two sub-problems.
- When the nonlocal sub-problem with Robin transmission condition is asymptotically compatible, the coupling framework preserves the asymptotic compatibility.
- The partitioned procedure passes the patch tests as long as the solution satisfies the chosen Robin transmission condition. In particular, when taking T^{NL} as the corresponding local operator T^{L} in the partitioned procedure for the overlapping case, the coupling framework passes up to cubic patch tests. On the contrary, in the partitioned procedure for the non-overlapping case, as in [157], the coupling framework simply passes the linear and quadratic patch tests only when the interface is flat.
- The partitioned procedure with the implicit coupling approach is energy preserving. However, the explicit coupling approach does not necessarily guarantee energy preservation.
- The partitioned procedure for the non-overlapping case can also be applied to general heterogeneous LtN coupling problems, i.e., where the local and nonlocal problems have different physical properties.

3.2.2 Applications and Results

In applications, the optimal Robin coefficients can be estimated either theoretically or numerically. In problems with relatively simple and/or structured domain settings, one can perform a Fourier decomposition of the solution and define an analytical reduction factor as the ratio between the semi-discretized solution errors of the current and previous iterations in the frequency space. Then, the optimal Robin coefficients can be obtained by minimizing the analytical reduction factor, as shown in [158]. There, the authors consider a LtN coupling for two-dimensional static/quasi-static mechanics problems, involving a nonlinear bond-based peridynamic model given by the prototype microelastic brittle (PMB) model [134] discretized with a meshfree method, coupled to a classical linear elasticity model (see (22)) discretized with the FEM. On a simple problem setting representing a plate under uniaxial tension, the optimal Robin coefficients are provided by reducing the coupling problem to a one-dimensional model problem and obtaining expressions for the reduction factor of the solution. The developed optimal Robin transmission condition is also applied to capture crack initiation and growth on a plate with a hole loaded with increasing tension.

For LtN coupling problems with general geometry and heterogeneous material properties, deriving the analytical expression of the reduction factor is generally not straightforward, and typically a numerical approximation has to be considered. In [157], LtN coupling in a diffusion problem for the non-overlapping case is studied. Using Robin transmission

conditions, the authors developed a stable explicit partitioned procedure, where the optimal Robin coefficients are obtained by minimizing the magnitude of the maximum eigenvalue of the discretized coupled system. When the time step satisfies the CFL condition $\Delta t \leqslant Ch^2$, where h is the spatial discretization size and C is a constant, the resulting partitioned procedure with optimal Robin coefficients is robust and capable of handling sub-domains with complicated geometries, as shown in Fig. 11. The numerical results on patch tests are shown in Fig. 12, where both the local and nonlocal sub-domains are two-dimensional squares and the interface Γ_v is a straight line segment. In Fig. 12, solutions along the domain center line are reported.

4 Atomistic-to-Continuum Type Coupling

4.1 Arlequin Method

The Arlequin method [14, 15] is a general energy-based engineering design tool for multi-scale modeling which superimposes multiple models and glues them to each other while partitioning and weighting the energies. In this section, we review the Arlequin approach for LtN coupling, following [71]. In that work, the authors employ the nonlocal elasticity model developed in [42, 43]. Here, for consistency with the rest of the paper, we adapt the formulation from [71] to couple the bond-based peridynamic model (18) (with the linear pairwise force function (19)) and classical linear elasticity (see (22)). For state-based peridynamics, the Arlequin method has been applied in [149].

4.1.1 Mathematical Formulation

We refer to Fig. 4 (bottom): the domain $\widehat{\Omega}$ is decomposed into $\overline{\Omega}_l$ and $\widehat{\Omega}_{nl}$ with an overlapping region $\overline{\Omega}_o := \overline{\Omega}_l \cap \widehat{\Omega}_{nl}$, whose volume has to be sufficiently large to ensure stability [12, 71]. The strain energy density of the system is defined in the following way: it equals the nonlocal strain energy density in $\Omega_{nl} \setminus \Omega_o$ and the local strain energy density in $\Omega_l \setminus \Omega_o$. In the overlapping region, Ω_o, the strain energy density is defined as a weighted combination of the strain energy densities of the two models using complementary weight functions. We introduce below, in a three-dimensional setting, the weak form of the system for the Arlequin formulation.

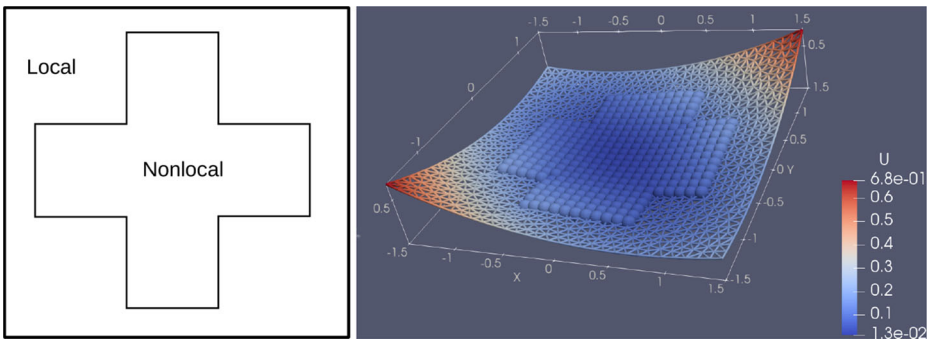

Fig. 11 Non-overlapping partitioned procedure for LtN coupling. Left: problem setting. Right: simulation result, where the blue spheres represent the nonlocal solution obtained with a meshfree solver and the triangular mesh represents the local solution obtained via a FEM solver

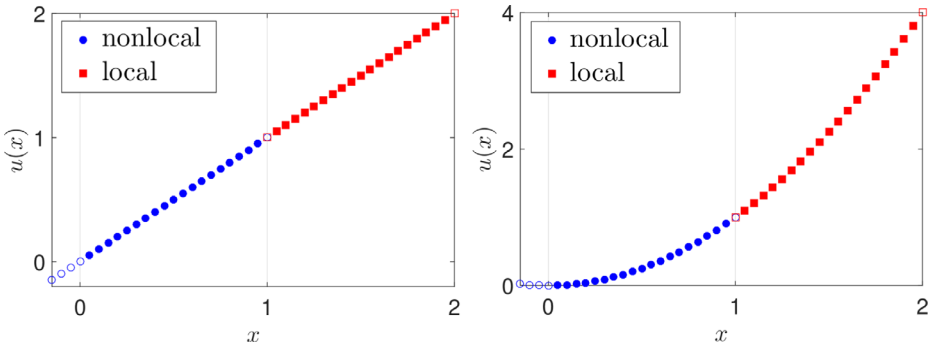

(a) Linear Patch Test (b) Quadratic Patch Test

Fig. 12 Patch tests for the non-overlapping partitioned procedure: linear (left) and quadratic (right). Nodes in the nonlocal sub-domain are represented by blue filled circles, whereas nodes in the nonlocal boundary (left physical nonlocal boundary and local-nonlocal interface) are represented by empty blue circles. Nodes in the local sub-domain are represented by red filled squares, whereas nodes on the local boundary (right physical local boundary and local-nonlocal interface) are represented by empty red squares

The functional spaces for the local model are defined as

$$W_1 := \left\{\mathbf{u} \in H^1\left(\overline{\Omega}_l\right) : \mathbf{u}(\mathbf{x}) = \mathbf{g}(\mathbf{x}) \text{ on } \Gamma_p\right\},$$
$$W_1^0 := \left\{\mathbf{v} \in H^1\left(\overline{\Omega}_l\right) : \mathbf{v}(\mathbf{x}) = \mathbf{0} \text{ on } \Gamma_p\right\}.$$

Given a function pair $(\mathbf{u}_1, \mathbf{v}_1) \in W_1 \times W_1^0$, we define a local weighted bilinear form:

$$a_1(\mathbf{u}_1, \mathbf{v}_1) := \int_{\Omega_l} \alpha_1(\mathbf{x}) \frac{4E}{5} \Big\{ (\nabla \cdot \mathbf{u}_1(\mathbf{x}))\,(\nabla \cdot \mathbf{v}_1(\mathbf{x})) + \frac{1}{2}\left(\nabla \mathbf{u}_1(\mathbf{x}) + \nabla \mathbf{u}_1^T(\mathbf{x})\right) : \left(\nabla \mathbf{v}_1(\mathbf{x}) + \nabla \mathbf{v}_1^T(\mathbf{x})\right) \Big\} d\mathbf{x}. \tag{30}$$

For the nonlocal model, we define the functional spaces $W_2 := \mathcal{S}^{\mathrm{PD}}(\widehat{\Omega}_{nl})$ and $W_2^0 := \mathcal{S}_c^{\mathrm{PD}}(\widehat{\Omega}_{nl})$. Given a function pair $(\mathbf{u}_2, \mathbf{v}_2) \in W_2 \times W_2^0$, we define a nonlocal weighted bilinear form:

$$a_2(\mathbf{u}_2, \mathbf{v}_2) := \frac{1}{4} \int_{\Omega_{nl}} \int_{B_\delta(\mathbf{x})} \alpha_2(\mathbf{x}, \mathbf{x}') \lambda(\|\mathbf{x}' - \mathbf{x}\|) \left(\mathbf{u}_2(\mathbf{x}') - \mathbf{u}_2(\mathbf{x})\right)^T \left((\mathbf{x}' - \mathbf{x}) \otimes (\mathbf{x}' - \mathbf{x})\right) \left(\mathbf{v}_2(\mathbf{x}') - \mathbf{v}_2(\mathbf{x})\right) d\mathbf{x}' d\mathbf{x}. \tag{31}$$

Here, $\alpha_1(\mathbf{x})$ and $\alpha_2(\mathbf{x}, \mathbf{x}')$ are complementary (see below) scalar-valued weight functions, which can be defined via a blending function $\beta(\mathbf{x})$ such as the one introduced in (2) and illustrated in Fig. 8a. We take $\alpha_1(\mathbf{x}) = 1 - \beta(\mathbf{x})$. In contrast to $\alpha_1(\mathbf{x})$, which is a one-point function, $\alpha_2(\mathbf{x}, \mathbf{x}')$ is a two-point function so that its definition is not unique. Nevertheless, as discussed in [12, 29], to reduce spurious effects $\alpha_2(\mathbf{x}, \mathbf{x}')$ can be chosen as a symmetric function (see [71]):

$$\alpha_2(\mathbf{x}, \mathbf{x}') = \beta\left(\frac{\mathbf{x} + \mathbf{x}'}{2}\right) \quad \forall \mathbf{x}, \mathbf{x}' \in \Omega. \tag{32}$$

Another standard choice of α_2 can be defined in an average sense [29, 111].

Next, we define the weak formulation of the local and nonlocal body forces, respectively. For $\mathbf{v}_1 \in W_1^0$, the local term is defined as

$$l_1(\mathbf{v}_1) := \int_{\Omega_l} \alpha_1(\mathbf{x})\mathbf{b}(\mathbf{x}) \cdot \mathbf{v}_1(\mathbf{x})\, d\mathbf{x}, \tag{33}$$

and, for $\mathbf{v}_2 \in W_2^0$, the nonlocal term is defined as

$$l_2(\mathbf{v}_2) := \int_{\Omega_{nl}} (1 - \alpha_1(\mathbf{x}))\mathbf{b}(\mathbf{x}) \cdot \mathbf{v}_2(\mathbf{x})\, d\mathbf{x}. \tag{34}$$

In order to couple the displacements of the local and nonlocal models in Ω_o, a weak compatibility between the kinematics of both models using Lagrange multipliers is enforced. The result is the following saddle point problem:

$$\begin{aligned}
&\text{Find } (\mathbf{u}_1, \mathbf{u}_2, \boldsymbol{\phi}) \in W_1 \times W_2 \times H^1(\Omega_o) \quad \text{such that} \\
&a_1(\mathbf{u}_1, \mathbf{v}_1) + C(\boldsymbol{\phi}, \mathbf{v}_1) = l_1(\mathbf{v}_1), && (35)\\
&a_2(\mathbf{u}_2, \mathbf{v}_2) - C(\boldsymbol{\phi}, \mathbf{v}_2) = l_2(\mathbf{v}_2), && (36)\\
&C(\boldsymbol{\psi}, \mathbf{u}_1 - \mathbf{u}_2) = 0, && (37)\\
&\text{for all } (\mathbf{v}_1, \mathbf{v}_2, \boldsymbol{\psi}) \in W_1^0 \times W_2^0 \times H^1(\Omega_o).
\end{aligned}$$

The bilinear form $C(\cdot, \cdot)$ describes the coupling and is defined, for any $(\boldsymbol{\psi}, \mathbf{v}) \in H^1(\Omega_o) \times \mathcal{S}^{\mathrm{PD}}(\Omega_o) \cap H^1$, as

$$C(\boldsymbol{\psi}, \mathbf{v}) := \int_{\Omega_o} (\kappa_0 \boldsymbol{\psi} \cdot \mathbf{v} + \kappa_1 \boldsymbol{\varepsilon}(\boldsymbol{\psi}) : \boldsymbol{\varepsilon}(\mathbf{v}))\, d\mathbf{x}, \tag{38}$$

where $\boldsymbol{\varepsilon}(\cdot)$ denotes the *infinitesimal strain tensor* $\boldsymbol{\varepsilon}(\mathbf{v}) := \frac{1}{2}\left(\nabla \mathbf{v} + \nabla \mathbf{v}^T\right)$. The coefficients $0 \leqslant \kappa_0, \kappa_1 \leqslant 1$ are non-negative coupling parameters. For example, $(\kappa_0, \kappa_1) = (1, 0)$ defines the L^2-norm coupling; $(\kappa_0, \kappa_1) = (0, 1)$ defines the H^1-seminorm coupling; and $(\kappa_0, \kappa_1) = (1, 1)$ is the H^1-norm coupling [17, 64, 65, 71].

Once the mixed formulation (35)–(37) is solved, we need to reconstruct a displacement $\mathbf{u}$ for the entire domain Ω, because $\mathbf{u}_1$ and $\mathbf{u}_2$ are only defined in Ω_l and $\widehat{\Omega}_{nl}$, respectively. One convenient reconstruction option is given as follows:

$$\mathbf{u}(\mathbf{x}) = \begin{cases} \mathbf{u}_1(\mathbf{x}) & \mathbf{x} \in \Omega_l \setminus \Omega_o, \\ \mathbf{u}_2(\mathbf{x}) & \mathbf{x} \in \Omega_{nl} \setminus \Omega_o, \\ \alpha_1(\mathbf{x})\mathbf{u}_1(\mathbf{x}) + (1 - \alpha_1(\mathbf{x}))\mathbf{u}_2(\mathbf{x}) & \mathbf{x} \in \Omega_o. \end{cases} \tag{39}$$

Properties Even though a mathematical analysis and a rigorous study of the influence of modeling choices of the Arlequin method (such as weight functions or size of the overlapping region) on the coupling quality are not available for LtN coupling in nonlocal mechanics, several references in the literature address properties of this technique when applied to other coupling problems (see, e.g., [12, 16, 29, 64]). Based on these references, we list here some general properties:

- If the coupling parameters defined in (38) satisfy $\kappa_0 \geqslant 0$ and $\kappa_1 > 0$, and the overlapping region Ω_o is sufficiently large, then the corresponding saddle point problem (35)–(38) is well-posed. However, for the L^2-norm coupling $(\kappa_0, \kappa_1) = (1, 0)$, the well-posedness is unclear.
- Since the condition for passing the linear patch test is only weakly imposed via (37), ghost forces cannot be completely removed in the overlapping region.

– The energy equivalence of this formulation depends on the choice of the weight functions α_1 and α_2, the size of the overlapping region Ω_o, and the choice of the Lagrange multiplier space [29, 64]. In some cases, the Arlequin model is not equivalent neither to the local model nor to the nonlocal model, even when homogeneous deformations are assumed. In fact, as pointed out in [29], with inappropriate choices of α_1, Ω_o, and (κ_0, κ_1), the Arlequin formulation may be not coercive.

The Time-Dependent Problem The Arlequin method has been used in many time-dependent applications, and the extension is straightforward (see, e.g., [12, 109, 149]). In particular, applications to dynamic LtN coupling in mechanics problems appear in [149]. However, such extension consists in solving the saddle point problem (35)–(37) at every time step, which limits its applicability due to high computational cost.

4.1.2 Applications and Results

In this section, as done in others below, we simply provide references to applications of the Arlequin method as the reproduction of numerical results is non-trivial.

In [71], the authors first apply the H^1-norm coupling with piece-wise linear weight functions to study a two-dimensional cantilever beam of isotropic homogeneous material. Their results show that the accuracy of Arlequin solutions is comparable with that of a fully nonlocal elasticity model. Next, they test a static cracked square plate using various options of (κ_0, κ_1). When the H^1-norm coupling with piece-wise linear weight functions is used, the strain distribution from the Arlequin approach agrees with the strain field, especially near the crack-tip, computed with the fully nonlocal model.

In [110], the authors use the Arlequin method to investigate a one-dimensional problem that consists of a collection of springs that exhibit a localized defect, resulting in a sudden change in the spring properties. They test the method and study its accuracy for several choices of coupling parameters. They prove that the Arlequin formulation is well-posed with both H^1-seminorm and H^1-norm couplings. Their numerical results also indicate that the method is sensitive to the location and size of the overlapping region, and they propose to utilize adaptive strategies, based on a posteriori error estimates, to identify them.

4.2 Morphing Method

The morphing method for LtN coupling was developed in [5, 6, 72, 90] based on a blending approach to morph the material properties of local and nonlocal sub-domains. The coupling formulation consists of a single unified model obtained by a transition (morphing) from local to nonlocal descriptions. More specifically, a hybrid model is introduced in the transition region or morphing zone, Ω_t (see Fig. 5), whose constitutive law changes gradually from a local to a nonlocal response. As a result, a single model with evolving material properties is defined on the whole domain and the equivalence of the energy of the system with the fully nonlocal energy is enforced in the morphing zone under homogeneous deformations [90].

4.2.1 Mathematical Formulation

We describe the morphing method for the coupling of the bond-based peridynamic model (18) (with the linear pairwise force function (19)) and the corresponding classical

linear elasticity model (22), following [90]. We note, however, that this technique has also been applied to more complex material models, including linear anisotropic bond-based peridynamic models [5] and a state-based peridynamic model [72].

The strain energy density of the linear bond-based peridynamic model is given by

$$W^{nl}(\mathbf{x}) = \tfrac{1}{4}\int_{B_\delta(\mathbf{0})} \lambda(\|\boldsymbol{\xi}\|)(\mathbf{u}(\mathbf{x}+\boldsymbol{\xi})-\mathbf{u}(\mathbf{x}))^T(\boldsymbol{\xi}\otimes\boldsymbol{\xi})(\mathbf{u}(\mathbf{x}+\boldsymbol{\xi})-\mathbf{u}(\mathbf{x}))d\boldsymbol{\xi}, \tag{40}$$

whereas the corresponding local strain energy density is given by

$$\begin{aligned} W^{l}(\mathbf{x}) &= \frac{4E}{5}\Big\{(\nabla\cdot\mathbf{u}(\mathbf{x}))\,(\nabla\cdot\mathbf{u}(\mathbf{x})) \\ &\qquad +\frac{1}{2}\Big(\nabla\mathbf{u}(\mathbf{x})+\nabla\mathbf{u}^T(\mathbf{x})\Big):\Big(\nabla\mathbf{u}(\mathbf{x})+\nabla\mathbf{u}^T(\mathbf{x})\Big)\Big\} \\ &= \frac{1}{2}\boldsymbol{\varepsilon}(\mathbf{x}):\mathcal{C}^l:\boldsymbol{\varepsilon}(\mathbf{x}), \end{aligned} \tag{41}$$

where $\mathcal{C}^l$ is the fourth-order elasticity tensor and $\boldsymbol{\varepsilon} := \frac{1}{2}(\nabla\mathbf{u}+\nabla\mathbf{u}^T)$ is the infinitesimal strain tensor. When considering an infinitesimal homogeneous deformation, we can define a local stiffness tensor $\mathcal{C}^0$ using (40) such that the strain energy density of the resultant local model is equal to the strain energy density of the nonlocal model, i.e.,

$$W^{nl}(\mathbf{x}) \approx \frac{1}{2}\boldsymbol{\varepsilon}(\mathbf{x}):\mathcal{C}^0:\boldsymbol{\varepsilon}(\mathbf{x}),$$

where $\mathcal{C}^0$ is given by (21). To define the morphing model, due to consistency requirements on the energy densities, we assume $\mathcal{C}^0 = \mathcal{C}^l$.

Given a blending or morphing function β, such as the one introduced in (2) and illustrated in Fig. 8b, the morphing model is fully defined by the following strain energy density:

$$\begin{aligned} W^{m}(\mathbf{x}) &= \frac{1}{2}\boldsymbol{\varepsilon}(\mathbf{x}):\mathcal{C}(\mathbf{x}):\boldsymbol{\varepsilon}(\mathbf{x}) \\ &\quad +\frac{1}{4}\int_{B_\delta(\mathbf{0})}\lambda(\|\boldsymbol{\xi}\|)\frac{\beta(\mathbf{x}+\boldsymbol{\xi})+\beta(\mathbf{x})}{2}(\mathbf{u}(\mathbf{x}+\boldsymbol{\xi})-\mathbf{u}(\mathbf{x}))^T(\boldsymbol{\xi}\otimes\boldsymbol{\xi})(\mathbf{u}(\mathbf{x}+\boldsymbol{\xi})-\mathbf{u}(\mathbf{x}))d\boldsymbol{\xi}, \end{aligned}$$

where

$$\mathcal{C}(\mathbf{x}) := (1-\beta(\mathbf{x}))\mathcal{C}^l + \int_{B_\delta(\mathbf{0})}\lambda(\|\boldsymbol{\xi}\|)\frac{\beta(\mathbf{x})-\beta(\mathbf{x}+\boldsymbol{\xi})}{4}\boldsymbol{\xi}\otimes\boldsymbol{\xi}\otimes\boldsymbol{\xi}\otimes\boldsymbol{\xi}d\boldsymbol{\xi}.$$

Note that, similar to (21), $\mathcal{C}(\mathbf{x})$ is a fully symmetric fourth-order tensor.

Properties The morphing method has the following properties:

- For $\mathbf{x}\in\Omega_l$, $\mathcal{C}(\mathbf{x}) = \mathcal{C}^l$ and $W^m(\mathbf{x}) = W^l(\mathbf{x})$.
- For $\mathbf{x}\in\Omega_{nl}$, $\mathcal{C}(\mathbf{x}) = 0$ and $W^m(\mathbf{x}) = W^{nl}(\mathbf{x})$.
- This method does not pass the linear patch test. In fact, u^{lin} (see Definition 1) does not satisfy the equilibrium equation throughout the morphing zone and nonzero ghost forces arise [90]. However, these ghost forces can be approximately corrected using exactly the same deadload correction approach used in AtC coupling methods [126]. Besides, the ghost force intensity decreases when using smoother morphing functions β or sufficiently large morphing zones. Moreover, ghost forces are localized to the morphing zone and vanish when $\delta\to 0$.

- For homogeneous deformations, the strain energy density of the morphing method is equivalent to both strain energy densities of the local and nonlocal models. Therefore, this method is considered energy preserving under homogeneous deformations [90].
- Even though there are a few theoretical studies regarding the morphing method for LtN coupling, this method has been studied as a type of blending for AtC coupling [83]. The corresponding operator is coercive with respect to the nonlocal energy norm with smooth morphing function β and sufficiently large morphing zone Ω_t [83].

The Time-Dependent Problem The extension of the morphing method to time-dependent problems is straightforward, even though the implementation of the model has been only demonstrated in static/quasi-static problems.

4.2.2 Applications and Results

In this section, we simply provide references to applications of the morphing method as the reproduction of numerical results is non-trivial. In [90] this strategy is applied to couple linear bond-based peridynamics with classical linear elasticity for isotropic materials. The authors investigate the ghost force intensity when using different morphing functions. They perform a one-dimensional analysis followed by numerical studies in one and two dimensions. The results suggest that the ghost forces are localized to the morphing zone and a smoother morphing function β reduces the maximum relative ghost force [90]. Follow-on two-dimensional simulations for a cracked square plate under both traction and shear demonstrate the effectiveness of the method, compared with a fully peridynamic simulation. Later on, in [6], the morphing method is combined with an adaptive algorithm that updates the nonlocal sub-domain based on damage progression. The resulting coupling framework is applied to three-dimensional quasi-static problems. In [72], the method is further extended to couple a linearized state-based peridynamic model and the corresponding classical linear elasticity model. For anisotropic materials, in [5], the authors introduce anisotropic nonlocal models based on spherical harmonic descriptions and present three-dimensional results.

4.3 Quasi-Nonlocal Method

The quasi-nonlocal (QNL) method is an energy-based coupling approach introduced in the context of AtC coupling. This method redefines the nonlocal energy via a "geometric reconstruction" scheme in the transition region and local sub-domain of a LtN coupling configuration, in such a way that the method is linearly patch-test consistent [91, 127, 150]. We point out that the idea of "geometric reconstruction" is not limited to AtC coupling of solids; similar coupling strategies in the literature have been applied, for example, in computational fluid dynamics (see, e.g., the review papers [2, 81]). Here, we focus on the QNL method for LtN coupling of one-dimensional diffusion models, following [56, 82].

4.3.1 Mathematical Formulation

We refer to Fig. 6 (top): without loss of generality, consider the domain $\widehat{\Omega} = [-1-\delta, 1]$. The domain is decomposed into four disjoint sub-domains: $\widehat{\Omega} = \overline{\Omega}_p \cup \overline{\Omega}_{nl} \cup \overline{\Omega}_t \cup \overline{\Omega}_l$, which include the left physical nonlocal boundary $\Omega_p = (-1-\delta, -1)$, the nonlocal sub-domain $\Omega_{nl} = (-1,\ x^*)$, the transition region $\Omega_t = (x^*,\ x^*+\delta)$, and the local sub-domain $\Omega_l = (x^*+\delta,\ 1)$. The right physical local boundary is $\Gamma_p = \{1\}$. Note that the interface

between the nonlocal sub-domain and the transition region occurs at x^* satisfying $x^* \in (-1+2\delta, 1-2\delta)$, and the transition region, Ω_t, has thickness δ.

The crucial step in the QNL formulation is the "geometric reconstruction" [124, 127, 150] of the directional distance $u(x') - u(x)$ in the definition of the energy. Because of difficulties arising from reconstructing geometries with corners in high dimensions, we limit the discussion to the one-dimensional case.

Note that the one-dimensional nonlocal diffusion energy density associated with the bond $\xi = x' - x$ is

$$\frac{1}{2}\gamma_\delta(x'-x)\big(u(x')-u(x)\big)^2, \tag{42}$$

where we assume a radially symmetric nonlocal diffusion kernel, i.e., $\gamma_\delta(\xi) = \gamma_\delta(|\xi|)$, which is also compactly supported. In the QNL method, such bond energy density is modified when the bond is entirely located outside the nonlocal sub-domain. Specifically, the nonlocal energy is redefined by substituting the directional distance $\big(u(x')-u(x)\big)$ with a path integral, such that the local energy density, $\frac{1}{2}|\frac{du}{dx}(x)|^2$, is equivalent to the nonlocal one for sufficiently smooth u. Thus, we have that (42) is replaced by

$$\frac{1}{2}\gamma_\delta(x'-x)\int_0^1 \left|\frac{du}{dx}\big(x+t(x'-x)\big)\right|^2 |x'-x|^2 dt. \tag{43}$$

The combined total energy of the QNL model with interface at x^* is

$$\begin{aligned} E_\delta^{\mathrm{QNL}}(u) \;=\; & \frac{1}{4}\iint\limits_{x\leqslant x^* \text{ or } x'\leqslant x^*} \gamma_\delta(|x'-x|)\big(u(x')-u(x)\big)^2\, dx'dx \\ & +\frac{1}{4}\iint\limits_{x>x^* \text{ and } x'>x^*} \gamma_\delta(|x'-x|)\int_0^1 \left|\frac{du}{dx}(x+t(x'-x))\right|^2 |x'-x|^2 dt\, dx'dx. \end{aligned} \tag{44}$$

The definition of the QNL coupling operator $\mathcal{L}^{\mathrm{QNL}}$ is obtained by taking the negative first variation of the total energy (44). We split it into three parts [56]:

I. For $x \in \Omega_{nl}$:

$$\mathcal{L}^{\mathrm{QNL}}u(x) \;=\; \int_{x'\in\widehat{\Omega}} \gamma_\delta(|x'-x|)\big(u(x')-u(x)\big)\,dx'. \tag{45}$$

II. For $x \in \Omega_t$:

$$\mathcal{L}^{\mathrm{QNL}}u(x) = \int_{x'<x^*} \gamma_\delta(|x'-x|)\big(u(x')-u(x)\big)\,dx' + \frac{d}{dx}\left(\omega_\delta(x)\frac{du}{dx}(x)\right), \tag{46}$$

where $\omega_\delta(x)$ is defined as

$$\omega_\delta(x) := \int_0^1 dt \int_{|\xi|<\frac{|x-x^*|}{t}} |\xi|^2\gamma_\delta(|\xi|)\,d\xi.$$

III. For $x \in \Omega_l$:

$$\mathcal{L}^{\mathrm{QNL}}u(x) = \frac{d^2u}{dx^2}(x). \tag{47}$$

Properties We summarize the properties of the QNL method, following [56]:

- The QNL operator is self-adjoint (i.e., symmetric) as it is derived from a combined total energy [27].
- The method passes the linear patch test.

- The operator is positive-definite and, hence, it is energy stable with respect to the QNL energy defined in (44) as well as L^2 stable with respect to the $L^2(\widehat{\Omega})$ norm.
- The formulation satisfies the weak maximum principle and therefore it is mass-conserving.
- The method is asymptotically compatible and the coupled solution converges as $\mathcal{O}(\delta)$ to the corresponding local solution.
- The combined total energy of the QNL model is equivalent to both the fully nonlocal energy and the fully local energy up to linear functions.

The Time-Dependent Problem The extension of the QNL method to time-dependent problems is straightforward. This follows from the fact that the QNL operator $\mathcal{L}^{\text{QNL}}$ is coercive on the entire domain $\widehat{\Omega}$ and, hence, it is stable and monotonic.

4.3.2 Applications and Results

Consider the one-dimensional domain $\widehat{\Omega} = [-\delta, \ 1]$ with interface at $x^* = 1/2$. The domain is decomposed into the sub-domains $\Omega_p = (-\delta, 0)$, $\Omega_{nl} = (0, \ 1/2)$, $\Omega_t = (1/2, \ 1/2 + \delta)$, and $\Omega_l = (1/2 + \delta, \ 1)$. Results are obtained with the first-order asymptotically compatible finite difference method introduced in [56]. We report results of linear and quadratic patch tests. In this case, the horizon is taken as $\delta = 1/50$ and the grid size is $h = 1/200$. Results are presented in Fig. 13 and demonstrate that, even though theoretically the QNL method is only linearly path-test consistent, numerically both linear and quadratic patch tests are well passed.

We now discuss the application of the QNL method in [56] to remove surface effects. As mentioned in Section 1, volume constraints for nonlocal models have to be prescribed in a layer surrounding the domain, where data are not available or are hard to access. Consequently, an ad hoc treatment of nonlocal boundaries often causes unphysical surface effects. In [56], the authors apply the QNL method to allow the prescription of classical local boundary conditions in a nonlocal problem. Specifically, they address the nonlocal boundary issue by coupling nonlocal and local models, being the latter placed in the nonlocal boundary region. Figure 14b shows the solution of a local-nonlocal-local (L-N-L)

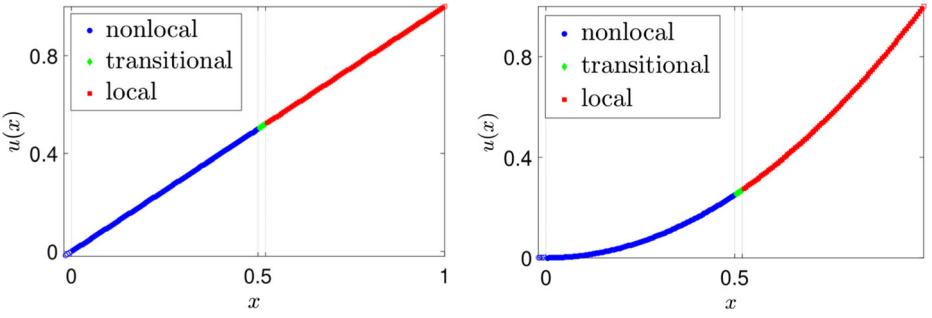

(a) Linear Patch Test (b) Quadratic Patch Test

Fig. 13 Patch tests for the quasi-nonlocal (QNL) method: linear (left) and quadratic (right). Nodes in the nonlocal sub-domain are represented by blue filled circles, whereas nodes in the left physical nonlocal boundary are represented by empty blue circles. Nodes in the local sub-domain are represented by red filled squares, whereas the node on the right physical local boundary is represented by an empty red square. Green diamonds represent nodes in the transition region described by the QNL model

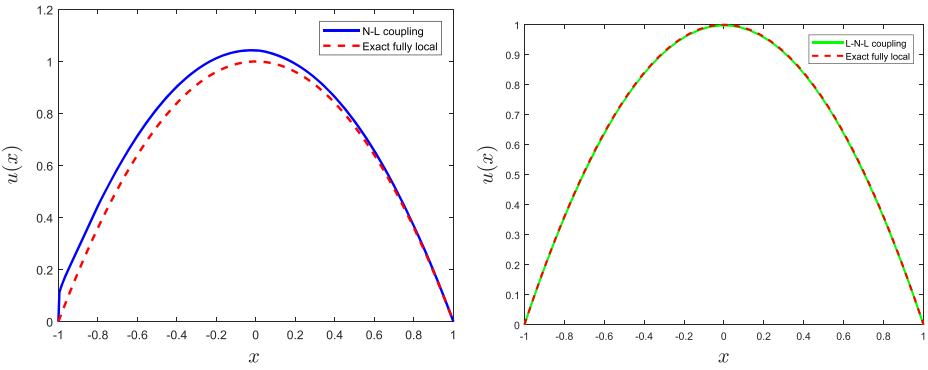

(a) Nonlocal-local coupling (b) Local-nonlocal-local coupling

Fig. 14 Application of the quasi-nonlocal method to impose classical local boundary conditions in a nonlocal problem. Left: nonlocal-local (N-L) coupling with a classical Dirichlet boundary condition extended to the left physical nonlocal boundary and a classical Dirichlet boundary condition imposed on the right physical local boundary. Right: local-nonlocal-local (L-N-L) coupling with classical Dirichlet boundary conditions imposed on both the left and right physical local boundaries

coupling with boundaries being treated in a fully classical way, whereas Fig. 14a shows the solution of a nonlocal-local (N-L) coupling by simply imposing a Dirichlet volume constraint $u(x) = 0$ in the left physical nonlocal boundary $\Omega_p = (-1-\delta, -1)$. In those two examples, the nonlocal diffusion kernel is chosen as $\gamma_\delta(\xi) = \frac{3}{\delta^3}\chi_{[-\delta,\delta]}(\xi)$ and the source is $f \equiv 1$. The L-N-L coupling has two interfaces located at $x^a = -\frac{1}{2}$ and $x^b = \frac{1}{2}$; the N-L coupling has one interface at $x^* = 0$. The horizon is $\delta = 0.2$ and the grid size is $h = 1/800$. We observe that the N-L coupling displays unphysical surface effects on the nonlocal side, whereas the L-N-L coupling eliminates those effects. Consequently, L-N-L coupling provides a way of imposing classical local boundary conditions in a nonlocal problem and helps avoiding the need of complicated extensions of local boundary conditions to nonlocal boundaries.

Remark 2 Finding an analytic geometric reconstruction formula becomes more difficult in higher dimensions. The nonlocal neighborhood, $B_\delta(\mathbf{x})$, becomes a disk (in two dimensions) or a ball (in three dimensions), making the intersections with the interface highly more complex. As a result, it is difficult to identify an explicit expression for the QNL method in a general setting (see discussions from [124]); even for a simple interface, such as a rectangular one, the exact formula is not yet available. In [74], the authors propose to adopt a least squares fitting procedure to find an approximation of this reconstruction; however, due to the inexactness of the approximation, the properties listed above no longer hold.

4.4 Blending Method

In this section, we discuss a force-based blending approach originally presented for one-dimensional linear bond-based peridynamic models in [118] and then extended to general bond-based peridynamic models in higher dimensions in [121]. Force-based blending is based on weighting governing equations via the introduction of a blending function. As discussed in [9], external or internal blending is possible. The former does not change the definitions of the reference models to be coupled, whereas the latter modifies their internal

force operators. In comparison with the morphing method discussed in Section 4.2, force-based blending does not necessarily have the physical interpretation of blending material properties. Force-based blending has been proposed in AtC coupling (see, e.g., [7, 57, 83, 84]). These AtC coupling methods are based on external blending and simply weight governing equations via the introduction of a blending function. In contrast, the approach from [118] is based on internal blending and arrives at a blended model through derivation from a single reference peridynamic model by only resorting to assumptions on the deformation. Here, as mentioned in Section 1.2, we employ the term "blending" to refer to force-based blending, because related methods, such as Arlequin and morphing, are called by their specific names.

4.4.1 Mathematical Formulation

We refer to Fig. 5: in this decomposition, the nonlocal sub-domain, Ω_{nl}, and the local sub-domain, Ω_l, do not overlap, but are separated by the transition region, Ω_t. A blending function $\beta(\mathbf{x})$, such as the one introduced in (2) and illustrated in Fig. 8b, is used to characterize the different sub-domains. The change in the blending function occurs within the so-called blending region, $\Omega_b \subset \Omega_t$, and normally takes a polynomial shape. Due to nonlocality, however, the influence of the variation in the blending function extends beyond the blending region and affects the entire transition region, which is given by $\Omega_t = \Omega_b \cup \mathcal{B}\Omega_b$.

The force-based blending approach presented here begins with a single reference bond-based peridynamic model given by (18) for all $\mathbf{x} \in \Omega$. Employing a symmetric combination of the blending function (2), the operator is first split into two complementary contributions, so that one of the two has nonzero support in regions of small smooth deformation. For that contribution, a linearization of the pairwise force function is used followed by a Taylor expansion of the displacement at any neighbor point $\mathbf{x}' \in B_\delta(\mathbf{x})$ around $\mathbf{x}$ up to second order, which leads to an expression connected to the local model. In the case of isotropy, the resulting blended operator is given by:

$$\begin{aligned}\mathcal{L}^b\mathbf{u}(\mathbf{x}) \;=\; & \int_{B_\delta(\mathbf{0})} \left(\frac{\beta(\mathbf{x})+\beta(\mathbf{x}+\boldsymbol{\xi})}{2}\right)\mathbf{f}(\boldsymbol{\eta},\boldsymbol{\xi})d\boldsymbol{\xi} \\ & -\frac{1}{2}\left[\int_{B_\delta(\mathbf{0})} \beta(\mathbf{x}+\boldsymbol{\xi})\lambda(\|\boldsymbol{\xi}\|)\xi_i\xi_j\xi_k d\boldsymbol{\xi}\right]\frac{\partial u_j}{\partial x_k}(\mathbf{x})\mathbf{e}_i \\ & -\frac{1}{2}\left[\int_{B_\delta(\mathbf{0})} \left(\frac{\beta(\mathbf{x})+\beta(\mathbf{x}+\boldsymbol{\xi})}{2}\right)\lambda(\|\boldsymbol{\xi}\|)\xi_i\xi_j\xi_k\xi_l d\boldsymbol{\xi}\right]\frac{\partial^2 u_j}{\partial x_k\partial x_l}(\mathbf{x})\mathbf{e}_i \\ & +\mathcal{C}_{ijkl}\frac{\partial^2 u_j}{\partial x_k\partial x_l}(\mathbf{x})\mathbf{e}_i, \end{aligned} \tag{48}$$

where $\mathcal{C}_{ijkl}$ are the components of the fourth-order elasticity tensor given by (21). We further used antisymmetry to simplify the term involving first-order derivatives of displacements.

Properties From (48), we have the following properties:

- For $\mathbf{x} \in \Omega_l$, $\mathcal{L}^b\mathbf{u}(\mathbf{x}) = \mathcal{L}^{\mathrm{CE}}\mathbf{u}(\mathbf{x})$ (see (22)).
- For $\mathbf{x} \in \Omega_{nl}$, $\mathcal{L}^b\mathbf{u}(\mathbf{x}) = \mathcal{L}^{\mathrm{PD}}\mathbf{u}(\mathbf{x})$ (see (18)).
- By construction, in the case of small deformations, the blended operator (48) is equivalent to the reference bond-based peridynamic operator (18) and the classical linear elasticity operator (22) for quadratic displacements. Therefore, the model automatically passes the linear and quadratic patch tests. Employing a higher-order Taylor expansion

up to third order instead would result in a blended model which also passes a cubic patch test.
– An error estimate provided in [121] shows that the blended operator (48) converges, in the limit of $\delta \to 0$ under suitable regularity assumptions, to the classical local operator (22) with an order of convergence of $\mathcal{O}(\delta)$. Employing a higher-order Taylor expansion up to third order in the derivation of the blended model would increase the order of convergence to $\mathcal{O}(\delta^2)$.

The Time-Dependent Problem The extension of the blending method to time-dependent problems is straightforward. In fact, in [118, 121] the blended model is presented based on equations of motion, even though the implementation of the model is demonstrated in static problems.

4.4.2 Applications and Results

Consider a one-dimensional domain $\widehat{\Omega} = [-\delta, 1]$ decomposed as in Fig. 5 (top) with $\delta = 0.05$. The blending region is chosen as $\Omega_b = (0.4, 0.6)$. We then have $\Omega_p = (-0.05, 0)$, $\Omega_{nl} = (0, 0.35)$, $\Omega_t = (0.35, 0.65)$, and $\Omega_l = (0.65, 1)$. We solve both linear and quadratic patch tests. The modeling choices and numerical implementation follow [118]. Specifically, a linear bond-based peridynamic model is used in Ω_{nl} with a meshfree discretization; classical linear elasticity is employed in Ω_l with a finite difference discretization; and the corresponding blended model given by (48) is implemented in Ω_t with a hybrid discretization, which features a meshfree discretization for integrals and a finite difference discretization for derivatives. A uniform grid with grid spacing $\Delta x = \delta/4$ is utilized. A piece-wise constant blending function is employed to demonstrate that no regularity is required for the blending function in this case; however, similar results are obtained for piece-wise linear and cubic blending functions. A Dirichlet volume constraint is imposed in the left physical nonlocal boundary Ω_p for the peridynamic model, whereas a Dirichlet boundary condition is imposed on the right physical local boundary $\Gamma_p = 1$ for the local model. The results are presented in Fig. 15 and demonstrate that the blended model passes the linear and quadratic patch tests.

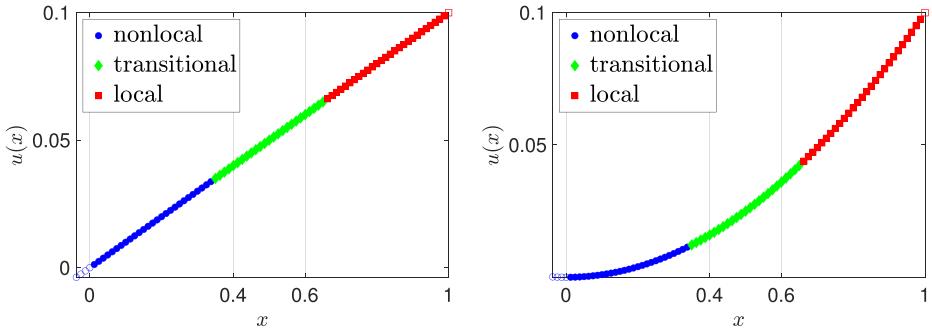

(a) Linear Patch Test (b) Quadratic Patch Test

Fig. 15 Patch tests for the blending method: linear (left) and quadratic (right). Nodes in the nonlocal sub-domain are represented by blue filled circles, whereas nodes in the left physical nonlocal boundary are represented by empty blue circles. Nodes in the local sub-domain are represented by red filled squares, whereas the node on the right physical local boundary is represented by an empty red square. Green filled diamonds represent nodes in the transition region described by the blended model

Additional static numerical examples demonstrating the performance of the blending method appear for one-dimensional problems in [118] and for two-dimensional problems in [121]. The one-dimensional studies include a point load case, where the sensitivity of the numerical results on the modeling choices, including the size of the nonlocal sub-domain where the point load is applied, the size of the blending region, the choice of blending function, and the horizon size, is investigated. Moreover, additional studies are conducted to quantify the effect of the location of the point load with respect to the coupling configuration as well as the speedup attained by employing a coarse discretization in the local sub-domain. Two-dimensional simulations include patch-test and point load examples as well as the deformation of a square plate subjected to both tensile and shear loading.

4.5 Splice Method

The splice method was originally presented for state-based peridynamics in [132] as a means to couple two peridynamic models with different horizons. Then, it was applied to LtN coupling by taking the horizon in one of the two peridynamic models to zero, so that the model can be effectively replaced by a classical local model. A methodology resembling the splice approach, formulated instead at the discrete level, was proposed to couple a discretized bond-based peridynamic model with a classical finite difference method in [151], with classical meshless methods in [128–130], and with classical FEs in [58, 159, 160]; the last one was extended to state-based peridynamics in [102]. Conceptually, the splice approach is probably the simplest LtN coupling method because each material point is described with a reference fully local or fully nonlocal model without the need of special coupling techniques.

4.5.1 Mathematical Formulation

Let a domain Ω be decomposed into two non-overlapping sub-domains Ω_{nl} and Ω_l, such that $\overline{\Omega} = \overline{\Omega_{nl}} \cup \overline{\Omega_l}$. These two sub-domains are connected by the interface Γ_v. This configuration resembles the one used in the partitioned procedure for the non-overlapping case and is illustrated in Fig. 6; here, however, the transition region Ω_t is empty.

We define the splice coupling operator as follows (see (15) and (12)):

$$\mathcal{L}^{\text{splice}}\mathbf{u}(\mathbf{x}) := \begin{cases} \int_{B_\delta(\mathbf{x})} \left\{ \underline{\mathbf{T}}[\mathbf{x}]\langle \mathbf{x}' - \mathbf{x} \rangle - \underline{\mathbf{T}}[\mathbf{x}']\langle \mathbf{x} - \mathbf{x}' \rangle \right\} d\mathbf{x}' & \mathbf{x} \in \Omega_{nl}, \\ \nabla \cdot \boldsymbol{\nu}^0(\mathbf{x}) & \mathbf{x} \in \Omega_l. \end{cases} \tag{49}$$

The basic idea is that each material point is represented by either a fully local or fully nonlocal model. Near the interface Γ_v, a point in Ω_{nl} interacts with points in Ω_l. While such points belong to a local sub-domain, from the perspective of a point in Ω_{nl} the interaction is described by a fully nonlocal model. A similar but reversed situation occurs after discretization for certain nodes in Ω_l that interact with some nodes in Ω_{nl}.

Properties

- Because each material point in the splice method is described by either a fully local or fully nonlocal model, and those models are consistent up to third-order polynomials, the splice method passes the linear, quadratic, and cubic patch tests.
- The asymptotic compatibility property of the splice method is inherited from the asymptotic compatibility of the reference nonlocal model with an order of convergence of $\mathcal{O}(\delta^2)$.

– The numerical implementation of the splice method is generally non-intrusive and only requires passing information about the deformation between the local and nonlocal sub-domains across Γ_v.

The Time-Dependent Problem The splice method is directly applicable to time-dependent problems, as demonstrated in [132].

4.5.2 Applications and Results

Consider a one-dimensional domain $\widehat{\Omega} = [-\delta, 1]$ with $\delta = 0.05$ decomposed into $\widehat{\Omega} = \overline{\Omega_p} \cup \overline{\Omega_{nl}} \cup \overline{\Omega_l}$, where $\Omega_p = (-0.05, 0)$, $\Omega_{nl} = (0, 0.5)$, and $\Omega_l = (0.5, 1)$. We solve both linear and quadratic patch tests. We employ a linear bond-based peridynamic model in Ω_{nl} discretized with a meshfree method and a classical linear elasticity model in Ω_l discretized with a finite difference method. A uniform grid with grid spacing $\Delta x = \delta/4$ is utilized. A Dirichlet volume constraint is imposed in the left physical nonlocal boundary for the peridynamic model, whereas a Dirichlet boundary condition is imposed on the right physical local boundary for the local model. The results are presented in Fig. 16 and demonstrate that the splice model passes the linear and quadratic patch tests.

Several numerical studies concerning the splice method have been carried out in the aforementioned references. In [132], the performance of the splice method is studied for a spall initiated by the impact of two brittle elastic plates. In [58], static numerical tests are performed, including one-dimensional linear and quadratic patch tests as well as three simulations in two dimensions, which concern the deformation of a plate undergoing rigid body motion, horizontal stretch, and shear. In [151], the method is proposed to mitigate wave dispersion in peridynamics, and crack propagation and branching in a pre-cracked plate under traction is simulated. Wave propagation in one and two dimensions as well as crack propagation in two and three dimensions are discussed in [159]; the crack propagation examples in two dimensions include a three-point bending test, the Kalthoff–Winkler experiment, and crack propagation and branching in a pre-cracked plate under traction, whereas in three dimensions an example is provided for a double cantilever beam test. Additional dynamic examples appear in [128] for a cantilever beam subjected to a periodic excitation as well as crack propagation and branching in a pre-cracked plate under traction. Advanced numerical

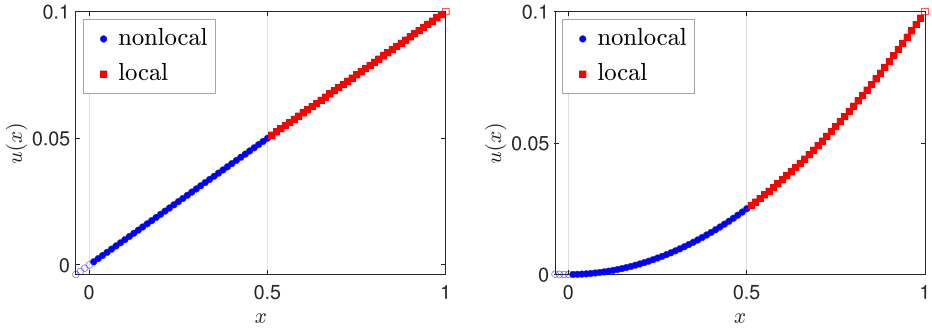

(a) Linear Patch Test (b) Quadratic Patch Test

Fig. 16 Patch tests for the splice method: linear (left) and quadratic (right). Nodes in the nonlocal sub-domain are represented by blue filled circles, whereas nodes in the left physical nonlocal boundary are represented by empty blue circles. Nodes in the local sub-domain are represented by red filled squares, whereas the node on the right physical local boundary is represented by an empty red square

examples concerning brittle failure analysis are given in [102], including the wedge-splitting test and the Brokenshire torsion experiment. Finally, in [130] a switching nodal technique that can be used for adaptivity is presented.

5 Varying Horizon Approaches

The concept of varying the horizon in a nonlocal model for LtN coupling purposes is motivated by the convergence of nonlocal models to local counterparts in the limit as $\delta \to 0$, under suitable regularity assumptions, as discussed in Sections 2.2.1 and 2.2.2. Early studies with variable horizon for adaptive refinement in peridynamics are presented in [21, 22]. A formulation allowing a spatially dependent horizon is introduced for nonlocal diffusion models in [120], where a LtN coupled problem is cast as a nonlocal interface problem and obtained by vanishing the horizon in one of two coupled sub-domains. The concept of smoothly varying the horizon is presented and analyzed in [132] and demonstrated for the coupling of two peridynamic models with different horizons. Later on, the shrinking horizon approach in nonlocal diffusion is analyzed for LtN coupling in [140, 144]. As demonstrated below, the shrinking horizon method is not linearly patch-test consistent. To overcome this issue, while allowing to spatially vary the horizon, the partial stress method is proposed in [132].

In this section, we begin by discussing the shrinking horizon method, which is related to the formulation in [120], based on [132, 140] in Section 5.1 followed by a description of the partial stress method presented in [132] in Section 5.2.

5.1 Shrinking Horizon Method

In [132] the idea of spatially varying the horizon in a peridynamic medium is discussed. Specifically, the notion of material homogeneity under a change in horizon is presented, resulting in the concept of *variable scale homogeneous* body. This provides an appropriate rescaling of the peridynamic force vector state, so that the corresponding strain energy density remains invariant with respect to changes in the horizon, under uniform deformations. In the related works in [140, 144], the authors discuss the validity of the nonlocal diffusion models with a shrinking horizon as the material points approach an interface, where the nonlocal models were localized and connected to local models on the other side, effectively resulting in a LtN coupling. The coercivity and the trace space of the corresponding energy functionals were discussed to guarantee the well-posedness of such nonlocal models with localization on the interface. The coupled problem can be solved as a whole system or using a classical non-overlapping domain decomposition method, where the nonlocal and local models are treated separately with suitable transmission conditions on the interface. The shrinking horizon method is an energy-based VH approach. This method does not pass the patch tests; however, the errors can be controlled by choosing the horizon function properly. Below, for brevity, we mainly discuss the formulation in the context of nonlocal diffusion, but make connections, where appropriate, to the analogue peridynamic formulation.

5.1.1 Mathematical Formulation

Let Ω_{nl} and Ω_l be two open domains in $\mathbb{R}^n$ that satisfy $\overline{\Omega_{nl}} \cap \overline{\Omega_l} = \Gamma \subset \mathbb{R}^{n-1}$, as illustrated in Fig. 7. In the shrinking horizon method, we generalize the kernel γ in (4) as

$$\gamma(\mathbf{x}', \mathbf{x}) = \mathcal{X}_{B_{\delta(\mathbf{x})}}(\mathbf{x}' - \mathbf{x})\, k(\mathbf{x}', \mathbf{x}), \tag{50}$$

where the horizon is now a spatially dependent function, $\delta(\mathbf{x})$, that decays to zero as $\mathbf{x}$ approaches Γ. The kernel $k(\mathbf{x}', \mathbf{x})$ is then properly scaled. For instance, the properly scaled kernels, in one dimension, in (9) now become

$$k(x', x) = \frac{3}{\delta^3(x)} \quad \text{and} \quad k(x', x) = \frac{2}{\delta^2(x)} \frac{1}{|x' - x|}. \tag{51}$$

Using properly scaled kernels, we can get Δu as the limit operator of $\mathcal{L}^{\mathrm{ND}} u$ by taking $\delta(\mathbf{x}) \to 0$ for every $\mathbf{x} \in \Omega_{nl}$, under suitable regularity assumptions.

In peridynamics, a related scaling of the peridynamic force vector state, which models a variable scale homogeneous body, is given by [132]

$$\widehat{\underline{\mathbf{T}}}(\underline{\mathbf{Y}}[\mathbf{x}], \mathbf{x})\langle \boldsymbol{\xi} \rangle = \frac{1}{(\delta(\mathbf{x}))^{1+n}} \widehat{\underline{\mathbf{T}}}_1(\underline{\mathbf{Y}}_1[\mathbf{x}]) \left\langle \frac{\boldsymbol{\xi}}{\delta(\mathbf{x})} \right\rangle, \tag{52}$$

where n is the spatial dimension, $\widehat{\underline{\mathbf{T}}}_1$ is a reference material model with a unit horizon, $\underline{\mathbf{Y}}$ is the deformation vector state (see (14)), and $\underline{\mathbf{Y}}_1$ is the reference deformation vector state defined by $\underline{\mathbf{Y}}_1\langle \mathbf{n} \rangle := \delta^{-1} \underline{\mathbf{Y}} \langle \delta \mathbf{n} \rangle$ with $\mathbf{n}$ a bond of length $\|\mathbf{n}\| \leqslant 1$.

A simple choice of the horizon function $\delta(\mathbf{x})$ is given by

$$\delta(\mathbf{x}) = \min(\delta, \operatorname{dist}(\mathbf{x}, \Gamma)) \tag{53}$$

with δ being the maximum value of $\delta(\mathbf{x})$. This choice of the horizon function is depicted in Fig. 7. In one dimension, the horizon function $\delta(\mathbf{x})$ given by (53) is a piece-wise linear function. However, numerical examples in Section 5.1.2 show that better horizon functions may be used in order to attain optimal order of convergence to the local limit as $\max_{\mathbf{x}} \delta(\mathbf{x}) \to 0$.

With the localization of the nonlocal interactions at the boundary Γ, it is shown in [144] that the corresponding nonlocal energy space $\mathcal{S}^{\mathrm{ND}}(\widehat{\Omega}_{nl})$ has $H^{1/2}(\Gamma)$ as the trace space on Γ, which is exactly the trace space of H^1 functions. As a consequence, we can define the combined energy space

$$\mathcal{W}(\widehat{\Omega}) = \{u \in \mathcal{S}(\widehat{\Omega}_{nl}) \cap H^1(\Omega_l) \,:\, u_- = u_+ \text{ on } \Gamma, u|_{\mathcal{B}\Omega} = 0\},$$

where $u_-(\mathbf{x}) := \lim_{\mathbf{y} \to \mathbf{x}, \mathbf{y} \in \Omega_{nl}} u(\mathbf{y})$ and $u_+(\mathbf{x}) := \lim_{\mathbf{y} \to \mathbf{x}, \mathbf{y} \in \Omega_l} u(\mathbf{y})$. The total energy of the shrinking horizon method is a combination of the nonlocal and local contributions given by

$$\begin{aligned} E(u, f) = & \frac{1}{4} \int_{\widehat{\Omega}_{nl}} \int_{\widehat{\Omega}_{nl}} \gamma(\mathbf{x}', \mathbf{x})((\mathcal{D}^* u)(\mathbf{x}', \mathbf{x}))^2 d\mathbf{x}' d\mathbf{x} + \frac{1}{2} \int_{\Omega_l} |\nabla u(\mathbf{x})|^2 d\mathbf{x} \\ & - \int_{\Omega} f(\mathbf{x}) u(\mathbf{x}) d\mathbf{x}, \end{aligned}$$

for any $u \in \mathcal{W}(\widehat{\Omega})$. The force balance equation is then the first variation of the total energy. The well-posedness of the coupled problem is guaranteed by the extension of the nonlocal Poincaré inequalities (Lemma 1) to the nonlocal space with variable horizon kernel γ given by (50).

Properties

- The shrinking horizon method is well-posed and energy stable for diffusion problems on general domains in all dimensions.
- There is no overlapping region between nonlocal and local sub-domains. Moreover, since the nonlocal and local energy functionals have the same trace space on the interface, one can use classical non-overlapping domain decomposition methods for solving the coupled problem.

- The method does not pass the patch tests. However, ghost forces can be controlled by using a smooth and slowly varying horizon function.
- The order of convergence of the solution of the coupled problem to the solution of the local problem as $\delta \to 0$ depends on the choice of the horizon function. For a piece-wise linear horizon function, the solution convergences at a rate of $\mathcal{O}(\delta)$. In contrast, with a smooth and slowly varying horizon function, e.g., the C^2 horizon function shown in Fig. 17a, the optimal order $\mathcal{O}(\delta^2)$ can be achieved.
- The total energy of the shrinking horizon method is equivalent to both the fully nonlocal energy and the fully local energy up to linear functions.

The Time-Dependent Problem The extension of the method to time-dependent problems is straightforward, even though the implementation has only been demonstrated in static problems. It would be interesting to see how the smooth and slowly varying horizon function can help reduce spurious effects, such as wave reflections, in a dynamic coupling problem.

5.1.2 Applications and Results

The shrinking horizon approach produces well-posed coupled models for a general horizon function $\delta(\mathbf{x})$ that gets localized at Γ, as shown in [140, 141]. However, the particular choices of the horizon function affect the convergence rate of the solutions as $\delta(= \max_{\mathbf{x}} \delta(\mathbf{x})) \to 0$. In [140], one-dimensional simulations are performed to illustrate that the solutions converge only at the order $\mathcal{O}(\delta)$ when using a piece-wise linear horizon function, as the one given by (53). The authors provide two remedies for increasing the order of convergence. The first one uses a specific auxiliary function, whereas the second one employs a smooth and slowly varying horizon function. Here, we only discuss the second approach; this approach was also discussed in [132] as a means to reduce ghost forces.

Figure 17a shows two choices of the horizon function $\delta(x)$ in one dimension, with one being a piece-wise linear function and the other one being a C^2 function. Since the method does not pass the linear patch test exactly, it generates ghost forces when the solution is a linear profile u^{lin} (see Definition 1). Figure 17b shows the ghost forces over the domain $\Omega = (-1, 1)$ using each of the horizon functions. It is clear that the case of a piece-wise linear horizon function generates a significantly larger magnitude of ghost forces around the

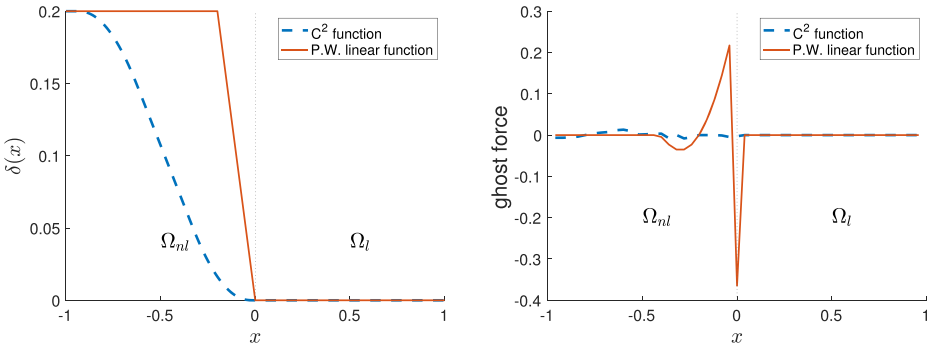

(a) Horizon functions (b) Ghost forces

Fig. 17 Left: examples of $\delta(x)$ in one dimension. The orange solid line represents a piece-wise linear horizon function and the blue dashed line represents a C^2 horizon function. Right: ghost forces in a linear patch test for the shrinking horizon method with the horizon functions from the left plot

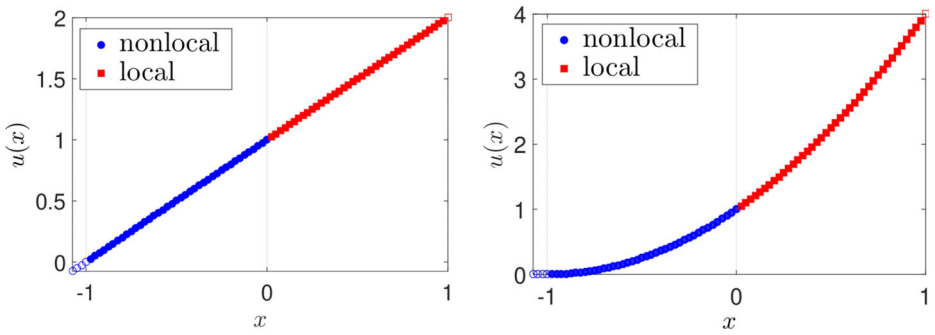

(a) Linear Patch Test (b) Quadratic Patch Test

Fig. 18 Patch tests for the shrinking horizon method with C^2 horizon function $\delta(x)$: linear (left) and quadratic (right). Nodes in the nonlocal sub-domain are represented by blue filled circles, whereas nodes in the left physical nonlocal boundary are represented by empty blue circles. Nodes in the local sub-domain are represented by red filled squares, whereas the node on the right physical local boundary is represented by an empty red square

interface between $\Omega_{nl} = (-1, 0)$ and $\Omega_l = (0, 1)$, compared with the case of a C^2 horizon function for which the ghost forces are less prominent. Moreover, it is observed in [140] that the ghost forces converge to zero everywhere as $\delta \to 0$ if the C^2 horizon function is used. Figure 18 further shows the linear and quadratic patch tests using the C^2 horizon function. In these tests, the largest horizon is $\delta = 0.1$ and the spatial mesh size is $\Delta x = 0.025$. The FEM with piece-wise linear basis functions is used for computing the numerical solution, since it is known to be an asymptotically compatible scheme for nonlocal variational problems [143, 145]. Although the coupled model does not pass the patch tests in theory, Fig. 18 shows that using the C^2 horizon function, the patch-test consistency could be attained approximately.

In addition to the above, numerical examples in [140] show that using the C^2 horizon function, the optimal order of convergence to the local limit can be achieved. In particular, the solution of the coupled problem converges to the solution of the local problem in the L^2 norm at the rate $\mathcal{O}(\delta^2)$. In contrast, using the piece-wise linear horizon function, one can only observe first-order convergence in the solution.

5.2 Partial Stress Method

As discussed in Section 5.1, the shrinking horizon method is not patch-test consistent, even though the ghost forces can be controlled by the regularity of the horizon function. In [132], this consideration led to the development of an alternative strategy to spatially vary the horizon, referred to as the partial stress method.

The proposition of the partial stress approach, which relates to Fig. 6, for LtN coupling is to reformulate the operator (12) in the transition region connecting local and nonlocal sub-domains, in a way that spatially varying the horizon in that region does not give rise to ghost forces under uniform deformations.

5.2.1 Mathematical Formulation

This method introduces a new tensor-valued function called the *partial stress* tensor,

$$\boldsymbol{\nu}^{\mathrm{ps}}(\mathbf{x}) := \int_{B_\delta(\mathbf{0})} \underline{\mathbf{T}}[\mathbf{x}]\langle \boldsymbol{\xi} \rangle \otimes \boldsymbol{\xi} \, d\boldsymbol{\xi}, \tag{54}$$

where $\underline{\mathbf{T}}$ is the force vector state from (12), and defines a corresponding *partial internal force density*,

$$\mathcal{L}^{\mathrm{ps}}\mathbf{u}(\mathbf{x}) := \nabla \cdot \boldsymbol{\nu}^{\mathrm{ps}}(\mathbf{x}). \tag{55}$$

In the case of simple (possibly non-homogeneous) materials (see (13)), the partial stress tensor can be expressed as

$$\boldsymbol{\nu}^{\mathrm{ps}}(\mathbf{x}) = \int_{B_\delta(\mathbf{0})} \widehat{\underline{\mathbf{T}}}(\underline{\mathbf{Y}}[\mathbf{x}], \mathbf{x})\langle \boldsymbol{\xi} \rangle \otimes \boldsymbol{\xi}\, d\boldsymbol{\xi}. \tag{56}$$

It is apparent that the partial stress tensor coincides with the collapsed stress tensor (see (16)) for $\underline{\mathbf{Y}}[\mathbf{x}] = \mathbf{F}(\mathbf{x})\underline{\mathbf{X}}$.

We now refer to Fig. 6: the domain Ω is decomposed into three disjoint sub-domains: $\overline{\Omega} = \overline{\Omega}_{nl} \cup \overline{\Omega}_t \cup \overline{\Omega}_l$, i.e., the nonlocal sub-domain, the transition region, and the local sub-domain. The partial stress coupled problem is given by

$$\begin{cases} -\displaystyle\int_{B_\delta(\mathbf{x})} \left\{ \underline{\mathbf{T}}[\mathbf{x}]\langle \mathbf{x}' - \mathbf{x} \rangle - \underline{\mathbf{T}}[\mathbf{x}']\langle \mathbf{x} - \mathbf{x}' \rangle \right\} d\mathbf{x}' = \mathbf{b}(\mathbf{x}) & \mathbf{x} \in \Omega_{nl}, \\ -\nabla \cdot \boldsymbol{\nu}^{\mathrm{ps}}(\mathbf{x}) = \mathbf{b}(\mathbf{x}) & \mathbf{x} \in \Omega_t, \\ -\nabla \cdot \boldsymbol{\nu}^{0}(\mathbf{x}) = \mathbf{b}(\mathbf{x}) & \mathbf{x} \in \Omega_l. \end{cases} \tag{57}$$

Properties Not many properties have been discussed for the partial stress method in the literature. Here, we simply summarize two properties from [132]:

- For a uniform deformation of a homogeneous body,
$$\boldsymbol{\nu}^{\mathrm{ps}} \equiv \boldsymbol{\nu}^0 \qquad \text{and} \qquad \nabla \cdot \boldsymbol{\nu}^{\mathrm{ps}} \equiv \nabla \cdot \boldsymbol{\nu}^0 \equiv \mathbf{0}.$$
- The partial stress tensor (54) and partial internal force density (55) converge, under suitable regularity assumptions, to the corresponding classical local counterparts, in the limit as $\delta \to 0$, as $\mathcal{O}(\delta)$, so the method is asymptotically compatible.

The Time-Dependent Problem The partial stress method was, in fact, only demonstrated in a dynamic setting in [132], where in conjunction with the splice method was applied to the study of a spall initiated by the impact of two brittle elastic plates.

5.2.2 Applications and Results

As described above, the partial stress method was only applied in [132] to a dynamic problem. We therefore omit the details here and refer the reader to that work.

6 Conclusions

This paper presents a review of the state of the art of local-to-nonlocal (LtN) coupling for nonlocal diffusion and nonlocal mechanics, specifically peridynamics, and provides a classification of different LtN coupling approaches (see Fig. 1). Following a description of various coupling configurations and a highlight of desired properties of a general LtN coupling strategy, we report different LtN coupling methods from the literature. For each method, we briefly present its mathematical formulation and properties, and we discuss relevant applications and numerical results.

Table 1 Summary of LtN coupling methods

Method	References	Section	Transition	Linear patch test	Formulation
Optimization-based	[34, 35, 39]	3.1	Overlap	Exact	Force-based
Partitioned procedure	[157, 158]	3.2	Overlap or Sharp	Exact*	Force-based
Arlequin	[71, 149]	4.1	Hybrid	Approximate	Energy-based
Morphing	[72, 90]	4.2	Hybrid	Approximate	Energy-based
Quasi-nonlocal	[56]	4.3	Hybrid	Exact	Energy-based
Blending	[118, 121]	4.4	Hybrid	Exact	Force-based
Splice	[132]	4.5	Sharp	Exact	Force-based
Shrinking horizon	[132, 140]	5.1	Variable horizon	Approximate	Energy-based
Partial stress	[132]	5.2	Variable horizon with partial stress	Exact	Force-based

The asterisk in the table indicates that the patch-test consistency for the partitioned procedure is exact up to certain conditions (see Section 3.2)

We observe that, while many features and challenges are shared by all methods, there exist some significant differences in the formulation and implementation of the different methods. For instance, we find that even though a LtN coupling configuration can generally be divided into a local sub-domain, a transition region, and a nonlocal sub-domain (as illustrated in Fig. 3), each coupling method treats the transition region in its own specific way. Some methods overlap local and nonlocal descriptions, some employ a hybrid representation, some reduce the transition region to a sharp interface, and some utilize a variable horizon with or without changing the nonlocal operator. This variation in the treatment of the transition region has both analytical and numerical implications. For instance, an overlapping approach is normally non-intrusive, whereas a hybrid technique is typically intrusive; the variable horizon method may or may not be intrusive, depending on the available nonlocal implementation. Another important property largely emphasized in this review is the ability of a coupling method to pass the patch test. Some coupling methods do pass it exactly for up to a certain polynomial order, whereas others only pass it approximately; the linear patch test is the most popular one. Finally, we recognize two major formulations for LtN coupling, energy-based and force-based. The energy-based formulation provides a natural setting to impose energy preservation; however, because such formulation requires energy minimization, it is more native to static problems and the extension to dynamic settings may not be practical. On the other hand, while force-based approaches normally equally apply to static and dynamic problems, they not always carry a well-defined energy functional. In Table 1, we outline the methods discussed in this review, indicating relevant references and sections, and summarize some of these properties.

We conclude by stating that the goal of this review is not to provide a preferred way to perform LtN coupling, but rather to broaden the perspective of the readers so that they can use this review as a guide for selecting the most appropriate method based on the characteristics of the problem at hand, available implementations, and accessible data.

Funding Information M. D'Elia was supported by Sandia National Laboratories (SNL), SNL is a multimission laboratory managed and operated by National Technology and Engineering Solutions of Sandia, LLC., a wholly owned subsidiary of Honeywell International, Inc., for the U.S. Department of Energy's National Nuclear Security Administration under contract DE-NA0003525. This material is based upon work supported by the U.S. Department of Energy, Office of Science, Office of Advanced Scientific Computing Research

under Award Number DE-SC-0000230927. This paper describes objective technical results and analysis. Any subjective views or opinions that might be expressed in the paper do not necessarily represent the views of the U.S. Department of Energy or the United States Government. X. Li was supported by NSF-DMS 1720245 and a UNC Charlotte faculty research grant. P. Seleson was supported by the Laboratory Directed Research and Development Program of Oak Ridge National Laboratory, managed by UT-Battelle, LLC, for the U. S. Department of Energy. This manuscript has been co-authored by UT-Battelle, LLC under Contract No. DE-AC05-00OR22725 with the U.S. Department of Energy. The United States Government retains and the publisher, by accepting the article for publication, acknowledges that the United States Government retains a non-exclusive, paid-up, irrevocable, world-wide license to publish or reproduce the published form of this manuscript, or allow others to do so, for United States Government purposes. The Department of Energy will provide public access to these results of federally sponsored research in accordance with the DOE Public Access Plan (http://energy.gov/downloads/doe-public-access-plan). X. Tian was supported by NSF-DMS-2044945. Y. Yu was supported by NSF-DMS 1753031 and the Lehigh faculty research grant.

References

1. Agwai A, Guven I, Madenci E (2012) Drop-shock failure prediction in electronic packages by using peridynamic theory. IEEE Transactions on Components, Packaging and Manufacturing Technology 2(3):439–447
2. Aidun CK, Clausen JR (2010) Lattice-Boltzmann method for complex flows. Annual Reviews 42:439–472
3. Alali B, Lipton R (2012) Multiscale dynamics of heterogeneous media in the peridynamic formulation. J Elast 106(1):71–103
4. Askari E (2008) Peridynamics for multiscale materials modeling. Journal of Physics: Conference Series, IOP Publishing 125(1):649–654
5. Azdoud Y, Han F, Lubineau G (2013) A morphing framework to couple non-local and local anisotropic continua. Int J Solids Struct 50(9):1332–1341
6. Azdoud Y, Han F, Lubineau G (2014) The morphing method as a flexible tool for adaptive local/non-local simulation of static fracture. Comput Mech 54(3):711–722
7. Badia S, Bochev P, Lehoucq R, Parks M, Fish J, Nuggehally MA, Gunzburger M (2007) A force-based blending model for atomistic-to-continuum coupling. International Journal for Multiscale Computational Engineering 5(5):387–406
8. Badia S, Nobile F, Vergara C (2008) Fluid-structure partitioned procedures based on Robin transmission conditions. J Comput Phys 227(14):7027–7051
9. Badia S, Parks M, Bochev P, Gunzburger M, Lehoucq R (2008) On atomistic-to-continuum coupling by blending. Multiscale Modeling & Simulation 7(1):381–406
10. Bakunin O (2008) Turbulence and Diffusion: Scaling Versus Equations. Springer-Verlag Berlin Heidelberg
11. Bates P, Chmaj A (1999) An integrodifferential model for phase transitions: stationary solutions in higher space dimensions. J Stat Phys 95:1119–1139
12. Bauman PT, Ben Dhia H, Elkhodja N, Oden JT, Prudhomme S (2008) On the application of the Arlequin method to the coupling of particle and continuum models. Comput Mech 42:511–530
13. Bažant ZP, Jirásek M (2002) Nonlocal integral formulations of plasticity and damage: survey of progress. J Eng Mech 128(11):1119–1149
14. Ben Dhia H (1998) Multiscale mechanical problems: the Arlequin method. Comptes Rendus de l'Academie des Sciences Series IIB Mechanics Physics Astronomy 12(326):899–904
15. Ben Dhia H (1999) Numerical modeling of multiscale problems: the Arlequin method. In: Proceedings of the First European Conference on Computational Mechanics
16. Ben Dhia H, Rateau G (2001) Mathematical analysis of the mixed Arlequin method. Comptes Rendus de Académie des Sciences- Series I - Mathematics 332:649–654
17. Ben Dhia H, Rateau G (2005) The Arlequin method as a flexible engineering design tool. Int J Numer Methods Eng 62:1442–1462
18. Benson D, Wheatcraft S, Meerschaert M (2000) Application of a fractional advection-dispersion equation. Water Resour Res 36(6):1403–1412
19. Bobaru F, Duangpanya M (2010) The peridynamic formulation for transient heat conduction. Int J Heat Mass Transfer 53(19-20):4047–4059
20. Bobaru F, Foster J, Geubelle P, Silling S (2016) Handbook of Peridynamic Modeling. Modern Mechanics and Mathematics. Taylor & Francis. CRC Press

21. Bobaru F, Ha YD (2011) Adaptive refinement and multiscale modeling in 2D peridynamics. International Journal for Multiscale Computational Engineering 9(6):635–660
22. Bobaru F, Yang M, Alves LF, Silling SA, Askari E, Xu J (2009) Convergence, adaptive refinement, and scaling in 1D peridynamics. Int J Numer Methods Eng 77(6):852–877
23. Bobaru F, Zhang G (2015) Why do cracks branch? A peridynamic investigation of dynamic brittle fracture. Int J Fract 196:59–98
24. Buades A, Coll B, Morel JM (2010) Image denoising methods: a new nonlocal principle. SIAM Rev 52:113–147
25. Bucur C, Valdinoci E (2016) Nonlocal Diffusion and Applications. Springer International Publishing
26. Burch N, D'Elia M, Lehoucq R (2014) The exit-time problem for a Markov jump process. The European Physical Journal, Special Topics 223:3257–3271
27. Caffarelli L, Chan CH, Vasseur A (2011) Regularity theory for parabolic nonlinear integral operators. J Am Math Soc 24:849–869
28. Capodaglio G, D'Elia M, Bochev P, Gunzburger M (2020) An energy-based coupling approach to nonlocal interface problems. Computers & Fluids 207:104593
29. Chamoin L, Prudhomme S, Ben Dhia H, Oden T (2010) Ghost forces and spurious effects in atomic-to-continuum coupling methods by the Arlequin approach. Int J Numer Methods Eng 83(8–9):1081–1113
30. Chen CK, Fife PC (2000) Nonlocal models of phase transitions in solids. Advances in Mathematical Sciences and Applications 10(2):821–849
31. Chen W, Gunzburger M, Hua F, Wang X (2011) A parallel Robin-Robin domain decomposition method for the Stokes-Darcy system. SIAM J Numer Anal 49(3):1064–1084
32. Curtin WA, Miller RE (2003) Atomistic/continuum coupling in computational materials science. Modelling Simul Mater Sci Eng 11:R33–R68
33. Dayal K, Bhattacharya K (2006) Kinetics of phase transformations in the peridynamic formulation of continuum mechanics. Journal of the Mechanics and Physics of Solids 54(9):1811–1842
34. D'Elia M, Bochev P (2014) Optimization-based coupling of nonlocal and local diffusion models. In: Lipton R (ed) Proceedings of the Fall 2014 Materials Research Society Meeting, MRS Symposium Proceedings. Cambridge University Press, Boston
35. D'Elia M, Bochev P (2021) Formulation, analysis and computation of an optimization-based local-to-nonlocal coupling method. Results in Applied Mathematics 9:100129
36. D'Elia M, De los Reyes J, Miniguano Trujillo A (2019) Bilevel parameter optimization for nonlocal image denoising models. arXiv:1912.02347
37. D'Elia M, Du Q, Gunzburger M, Lehoucq R (2017) Nonlocal convection-diffusion problems on bounded domains and finite-range jump processes. Computational Methods in Applied Mathematics 17:707–722
38. D'Elia M, Gunzburger M, Vollmann C (2021) A cookbook for approximating Euclidean balls and for quadrature rules in finite element methods for nonlocal problems. Mathematical Models and Methods in Applied Sciences 31(08):1505–1567
39. D'Elia M, Perego M, Bochev P, Littlewood D (2016) A coupling strategy for nonlocal and local diffusion models with mixed volume constraints and boundary conditions. Computers & Mathematics with Applications 71(11):2218–2230
40. D'Elia M, Tian X, Yu Y (2020) A physically-consistent, flexible and efficient strategy to convert local boundary conditions into nonlocal volume constraints. SIAM Journal of Scientific Computing 42(4):1935–1949
41. Di Paola M, Failla G, Pirrotta A, Sofi A, Zingales M (2013) The mechanically based non-local elasticity: an overview of main results and future challenges. Philosophical Transactions of the Royal Society A 371(1993):20120433
42. Di Paola M, Failla G, Zingales M (2009) Physically-based approach to the mechanics of strong nonlocal linear elasticity theory. J Elast 97:103–130
43. Di Paola M, Failla G, Zingales M (2010) The mechanically-based approach to 3D non-local linear elasticity theory: long-range central interactions. Int J Solids Struct 47:2347–2358
44. Diehl P, Prudhomme S, Lévesque M (2019) A review of benchmark experiments for the validation of peridynamics models. J Peridyn Nonlocal Model 1:14–35
45. Discacciati M, Gervasio P, Quarteroni A (2013) The interface control domain decomposition (ICDD) method for elliptic problems. SIAM J Control Optim 51(5):3434–3458
46. Discacciati M, Quarteroni A, Valli A (2007) Robin-Robin domain decomposition methods for the Stokes-Darcy coupling. SIAM J Numer Anal 45(3):1246–1268
47. Dorduncu M, Barut A, Madenci E, Phan ND (2017) Peridynamic augmented XFEM. In: 58th AIAA/ASCE/AHS/ASC Structures, Structural Dynamics, and Materials Conference. AIAA, pp 2017–0656

48. Douglas J, Huang CS (1997) An accelerated domain decomposition procedure based on Robin transmission conditions. BIT Numerical Mathematics 37(3):678–686
49. Du Q (2001) Optimization based nonoverlapping domain decomposition algorithms and their convergence. SIAM J Numer Anal 39(3):1056–1077
50. Du Q (2019) Nonlocal modeling, analysis, and computation, CBMS-NSF Conference Series in Applied Mathematics, vol. 94 SIAM
51. Du Q, Engquist B, Tian X (2020) Multiscale modeling, homogenization and nonlocal effects: mathematical and computational issues. Contemporary Mathematics 754:115–140, 75 Years of Mathematics of Computation, AMS
52. Du Q, Gunzburger M, Lehoucq R, Zhou K (2012) Analysis and approximation of nonlocal diffusion problems with volume constraints. SIAM Rev 54(4):667–696
53. Du Q, Gunzburger M, Lehoucq R, Zhou K (2013) Analysis of the volume-constrained peridynamic Navier equation of linear elasticity. J Elast 113(2):193–217
54. Du Q, Gunzburger M, Lehoucq RB, Zhou K (2013) A nonlocal vector calculus, nonlocal volume–constrained problems, and nonlocal balance laws. Mathematical Models and Methods in Applied Sciences 23(03):493–540
55. Du Q, Gunzburger MD (2000) A gradient method approach to optimization-based multidisciplinary simulations and nonoverlapping domain decomposition algorithms. SIAM J Numer Anal 37(5):1513–1541
56. Du Q, Li XH, Lu J, Tian X (2018) A quasi-nonlocal coupling method for nonlocal and local diffusion models. SIAM J Numer Anal 56:1386–1404
57. Fish J, Nuggehally MA, Shephard MS, Picu CR, Badia S, Parks ML, Gunzburger M (2007) Concurrent AtC coupling based on a blend of the continuum stress and the atomistic force. Comput Methods Appl Mech Eng 196:4548–4560
58. Galvanetto U, Mudric T, Shojaei A, Zaccariotto M (2016) An effective way to couple FEM meshes and peridynamics grids for the solution of static equilibrium problems. Mech Res Commun 76:41–47
59. Gerstle W, Sau N, Silling S (2005) Peridynamic modeling of plain and reinforced concrete structures. In: SMIRT18: 18th Int. Conf. Struct. Mech. React. Technol., Beijing
60. Gervasio P, Lions JL, Quarteroni A (2001) Heterogeneous coupling by virtual control methods. Numer Math 90:241–264
61. Giannakeas IN, Papathanasiou TK, Bahai H (2019) Wave reflection and cut-off frequencies in coupled FE-peridynamic grids. Int J Numer Methods Eng 120:9–55
62. Giannakeas IN, Papathanasiou TK, Fallah AS, Bahai H (2020) Coupling XFEM and peridynamics for brittle fracture simulation-part I: feasibility and effectiveness. Comput Mech 66:103–122
63. Gilboa G, Osher S (2007) Nonlocal linear image regularization and supervised segmentation. Multiscale Modeling and Simulation 6:595–630
64. Guidault PA, Belytschko T (2007) On the l^2 and the h^1 couplings for an overlapping domain decomposition method using Lagrange multipliers. Int J Numer Methods Eng 70:322–350
65. Guidault PA, Belytschko T (2009) Bridging domain methods for coupled atomistic-continuum models with l^2 or h^1 couplings. Int J Numer Methods Eng 77:1566–1592
66. Gunzburger M, Lehoucq R (2010) A nonlocal vector calculus with application to nonlocal boundary value problems. Multiscale Modeling & Simulation 8(5):1581–1598
67. Gunzburger MD, Heinkenschloss M, Lee HK (2000) Solution of elliptic partial differential equations by an optimization-based domain decomposition method. Appl Math Comput 113(2-3):111–139
68. Gunzburger MD, Lee HK (2000) An optimization-based domain decomposition method for the Navier-Stokes equations. SIAM J Numer Anal 37(5):1455–1480
69. Gunzburger MD, Peterson JS, Kwon H (1999) An optimization based domain decomposition method for partial differential equations. Computers & Mathematics with Applications 37(10):77–93
70. Ha YD, Bobaru F (2010) Studies of dynamic crack propagation and crack branching with peridynamics. Int J Fract 162:229–244
71. Han F, Lubineau G (2012) Coupling of nonlocal and local continuum models by the Arlequin approach. Int J Numer Methods Eng 89(6):671–685
72. Han F, Lubineau G, Azdoud Y, Askari A (2016) A morphing approach to couple state-based peridynamics with classical continuum mechanics. Computer Methods in Applied Mechanics and Engineering 301:336–358
73. Jenabidehkordi A, Rabczuk T (2019) The multi-horizon peridynamics. CMES-Computer Modeling in Engineering & Sciences 121(2):493–500
74. Jiang F, Shen Y (2018) Mapped displacement discontinuity method: numerical implementation and analysis for crack problems. Journal of Shanghai Jiaotong University (Science) 23:158–165
75. Jirásek M. (2004) Nonlocal theories in continuum mechanics. Acta Polytechnica 44(5-6):16–34

76. Katiyar A, Agrawal S, Ouchi H, Seleson P, Foster JT, Sharma MM (2020) A general peridynamics model for multiphase transport of non-Newtonian compressible fluids in porous media. J Comput Phys 402:109075
77. Katiyar A, Foster JT, Ouchi H, Sharma MM (2014) A peridynamic formulation of pressure driven convective fluid transport in porous media. J Comput Phys 261:209–229
78. Kilic B, Madenci E (2010) Coupling of peridynamic theory and the finite element method. J Mech Mater Struct 5(5):707–733
79. Kulkarni S, Tabarraei A (2018) An analytical study of wave propagation in a peridynamic bar with nonuniform discretization. Eng Fract Mech 190:347–366
80. Le QV, Bobaru F (2018) Surface corrections for peridynamic models in elasticity and fracture. Comput Mech 61(4):499–518
81. Li S, Liu WK (2002) Meshfree and particle methods and their applications. Applied Mechanics Review 55(1):1–34
82. Li XH, Lu J (2017) Quasi-nonlocal coupling of nonlocal diffusions. SIAM J Numer Anal 55:2394–2415
83. Li XH, Luskin M, Ortner C (2012) Positive definiteness of the blended force-based quasicontinuum method. Multiscale Modeling & Simulation 10(3):1023–1045
84. Li XH, Luskin M, Ortner C, Shapeev AV (2014) Theory-based benchmarking of the blended force-based quasicontinuum method. Comput Methods Appl Mech Eng 268:763–781
85. Littlewood DJ (2015) Roadmap for peridynamic software implementation. Report SAND2015-9013, Sandia National Laboratories, Albuquerque, NM and Livermore, CA
86. Littlewood DJ, Silling SA, Mitchell JA, Seleson PD, Bond SD, Parks ML, Turner DZ, Burnett DJ, Ostien J, Gunzburger M (2015) Strong local-nonlocal coupling for integrated fracture modeling. Report SAND2015-7998, Sandia National Laboratories, Albuquerque, NM and Livermore, CA
87. Liu S, Fang G, Liang J, Lv D (2020) A coupling model of XFEM/peridynamics for 2D dynamic crack propagation and branching problems. Theoretical and Applied Fracture Mechanics 108:102573
88. Liu W, Hong JW (2012) A coupling approach of discretized peridynamics with finite element method. Computer Methods in Applied Mechanics and Engineering 245–246:163–175
89. Lou Y, Zhang X, Osher S, Bertozzi A (2010) Image recovery via nonlocal operators. J Sci Comput 42:185–197
90. Lubineau G, Azdoud Y, Han F, Rey C, Askari A (2012) A morphing strategy to couple non-local to local continuum mechanics. Journal of the Mechanics and Physics of Solids 60(6):1088–1102
91. Luskin M, Ortner C (2013) Atomistic-to-continuum coupling. Acta Numerica 22:397–508
92. Macek RW, Silling SA (2007) Peridynamics via finite element analysis. Finite Elem Anal Des 43(15):1169–1178
93. Mathew T (2008) Domain Decomposition Methods for the Numerical Solution of Partial Differential Equations, vol 61. Springer Science & Business Media, Berlin
94. Meerschaert MM, Sikorskii A (2012) Stochastic Models for Fractional Calculus, vol. 43. De Gruyter
95. Mengesha T, Du Q (2013) Analysis of a scalar nonlocal peridynamic model with a sign changing kernel. Discrete and Continuous Dynamical Systems - B 18(5):1415–1437
96. Mengesha T, Du Q (2014) The bond-based peridynamic system with Dirichlet-type volume constraint. Proceedings of the Royal Society of Edinburgh Section A: Mathematics 144(1):161–186
97. Mengesha T, Du Q (2014) Nonlocal constrained value problems for a linear peridynamic Navier equation. J Elast 116(1):27–51
98. Metzler R, Klafter J (2000) The random walk's guide to anomalous diffusion: a fractional dynamics approach. Phys Rep 339(1):1–77
99. Metzler R, Klafter J (2004) The restaurant at the end of the random walk: recent developments in the description of anomalous transport by fractional dynamics. Journal of Physics A: Mathematical and General 37(31):161–208
100. Miller R, Tadmor E (2009) A unified framework and performance benchmark of fourteen multiscale atomistic/continuum coupling methods. Model Simul Mater Sci Eng 17:053001
101. Neuman SP, Tartakovsky DM (2009) Perspective on theories of non-Fickian transport in heterogeneous media. Adv Water Resour 32:670–680
102. Ni T, Zaccariotto M, Zhu QZ, Galvanetto U (2021) Coupling of FEM and ordinary state-based peridynamics for brittle failure analysis in 3D. Mech Adv Mater Struct 28(9):875–890
103. Nicely C, Tang S, Qian D (2018) Nonlocal matching boundary conditions for non-ordinary peridynamics with correspondence material model. Comput Methods Appl Mech Eng 338:463–490
104. Nikpayam J, Kouchakzadeh MA (2019) A variable horizon method for coupling meshfree peridynamics to FEM. Comput Methods Appl Mech Eng 355:308–322
105. Olson D, Bochev P, Luskin M, Shapeev A (2014) Development of an optimization-based atomistic-to-continuum coupling method. In: Lirkov I, Margenov S, Waśniewski J (eds) Proceedings of LSSC 2013, Lecture Notes in Computer Science. Springer, Berlin, Heidelberg

106. Olson D, Bochev P, Luskin M, Shapeev A (2014) An optimization-based atomistic-to-continuum coupling method. SIAM J Numer Anal 52(4):2183–2204
107. Oterkus E, Madenci E, Weckner O, Silling S, Bogert P, Tessler A (2012) Combined finite element and peridynamic analyses for predicting failure in a stiffened composite curved panel with a central slot. Compos Struct 94(3):839–850
108. Pang G, D'Elia M, Parks M, Karniadakis GE (2020) nPINNs: nonlocal physics-informed neural networks for a parametrized nonlocal universal Laplacian operator. Algorithms and applications. J Comput Phys 422:109760
109. Pfaller S, Possart G, Steinmann P, Rahimi M, Böhm MC, Müller-Plathe F (2013) Molecular dynamics meets finite elements: an approach for coupled simulations of nanocomposites. In: Müser MH, Sutmann G, Winkler RG (eds) Hybrid particle continuum methods in computational materials physics, Publication Series of the John von Neumann Institute for Computing (NIC). Forschungszentrum Jülich GmbH
110. Prudhomme S, Ben Dhia H, Bauman P, Elkhodja N, Oden J (2008) Computational analysis of modeling error for the coupling of particle and continuum models by the Arlequin method. Comput Methods Appl Mech Eng 197:3399–3409
111. Prudhomme S, Chamoin L, Ben Dhia H, Bauman PT (2009) An adaptive strategy for the control of modeling error in two-dimensional atomic-to-continuum coupling simulations. Comput Methods Appl Mech Eng 198:1887–1901
112. Quarteroni A, Valli A (1999) Domain Decomposition Methods for Partial Differential Equations. Oxford University Press, London
113. Ren H, Zhuang X, Cai Y, Rabczuk T (2016) Dual-horizon peridynamics. Int J Numer Methods Eng 108(12):1451–1476
114. Ren H, Zhuang X, Rabczuk T (2017) Dual-horizon peridynamics: a stable solution to varying horizons. Comput Methods Appl Mech Eng 318:762–782
115. Schekochihin AA, Cowley SC, Yousef TA (2008) MHD turbulence: nonlocal, anisotropic, nonuniversal? In: IUTAM Symposium on Computational Physics and new Perspectives in Turbulence. Springer, Dordrecht, pp 347–354
116. Schumer R, Benson D, Meerschaert M, Baeumer B (2003) Multiscaling fractional advection-dispersion equations and their solutions. Water Resour Res 39(1):1022–1032
117. Schumer R, Benson D, Meerschaert M, Wheatcraft S (2001) Eulerian derivation of the fractional advection-dispersion equation. J Contam Hydrol 48:69–88
118. Seleson P, Beneddine S, Prudhomme S (2013) A force-based coupling scheme for peridynamics and classical elasticity. Comput Mater Sci 66:34–49
119. Seleson P, Gunzburger M (2010) Bridging methods for atomistic-to-continuum coupling and their implementation. Communications in Computational Physics 7(4):831–876
120. Seleson P, Gunzburger M, Parks ML (2013) Interface problems in nonlocal diffusion and sharp transitions between local and nonlocal domains. Comput Methods Appl Mech Eng 266:185–204
121. Seleson P, Ha YD, Beneddine S (2015) Concurrent coupling of bond-based peridynamics and the Navier equation of classical elasticity by blending. International Journal for Multiscale Computational Engineering 13(2):91–113
122. Seleson P, Littlewood DJ (2016) Convergence studies in meshfree peridynamic simulations. Computers & Mathematics with Applications 71(11):2432–2448
123. Seleson PD (2010) Peridynamic multiscale models for the mechanics of materials: constitutive relations, upscaling from atomistic systems, and interface problems. The Florida State University
124. Shapeev AV (2012) Consistent energy-based atomistic/continuum coupling for two-body potentials in one and two dimensions. Multiscale Modeling and Simulation 9:905–932
125. Shen F, Yu Y, Zhang Q, Gu X (2020) Hybrid model of peridynamics and finite element method for static elastic deformation and brittle fracture analysis. Engineering Analysis with Boundary Elements 113:17–25
126. Shenoy VB, Miller R, Tadmor E, Rodney D, Phillips R, Ortiz M (1999) An adaptive methodology for atomic scale mechanics: the quasicontinuum method. Journal of the Mechanics and Physics of Solids 47:611–642
127. Shimokawa T, Mortensen JJ, Schiotz J, Jacobsen KW (2004) Matching conditions in the quasicontinuum method: Removal of the error introduced at the interface between the coarse-grained and fully atomistic regions. Physics Review B 69:214104
128. Shojaei A, Mudric T, Zaccariotto M, Galvanetto U (2016) A coupled meshless finite point/peridynamic method for 2D dynamic fracture analysis. Int J Mech Sci 119:419–431
129. Shojaei A, Zaccariotto M, Galvanetto U (2016) On the coupling of peridynamics with a meshless method based on classical elasticity. In: ASME 2016 International Mechanical Engineering Congress and Exposition. American Society of Mechanical Engineers Digital Collection

130. Shojaei A, Zaccariotto M, Galvanetto U (2017) Coupling of 2D discretized peridynamics with a meshless method based on classical elasticity using switching of nodal behaviour. Eng Comput 34(5):1334–1366
131. Silling S (2000) Reformulation of elasticity theory for discontinuities and long-range forces. Journal of the Mechanics and Physics of Solids 48:175–209
132. Silling S, Littlewood D, Seleson P (2015) Variable horizon in a peridynamic medium. J Mech Mater Struct 10(5):591–612
133. Silling SA (2010) Linearized theory of peridynamic states. J Elast 99(1):85–111
134. Silling SA, Askari E (2005) A meshfree method based on the peridynamic model of solid mechanics. Computers & Structures 83(17-18):1526–1535
135. Silling SA, Epton M, Weckner O, Xu J, Askari E (2007) Peridynamic states and constitutive modeling. J Elast 88(2):151–184
136. Silling SA, Lehoucq RB (2008) Convergence of peridynamics to classical elasticity theory. J Elast 93:13–37
137. Sun W, Fish J (2019) Superposition-based coupling of peridynamics and finite element method. Comput Mech 64(1):231–248
138. Sun W, Fish J, Zhang G (2020) Superposition of non-ordinary state-based peridynamics and finite element method for material failure simulations. Meccanica 55:681–699
139. Tao Y, Tian X, Du Q (2017) Nonlocal diffusion and peridynamic models with Neumann type constraints and their numerical approximations. Appl Math Comput 305:282–298
140. Tao Y, Tian X, Du Q (2019) Nonlocal models with heterogeneous localization and their application to seamless local-nonlocal coupling. Multiscale Modeling & Simulation 17(3):1052–1075
141. Tian X (2017) Nonlocal models with a finite range of nonlocal interactions. Columbia University
142. Tian X, Du Q (2013) Analysis and comparison of different approximations to nonlocal diffusion and linear peridynamic equations. SIAM J Numer Anal 51(6):3458–3482
143. Tian X, Du Q (2014) Asymptotically compatible schemes and applications to robust discretization of nonlocal models. SIAM J Numer Anal 52:1641–1665
144. Tian X, Du Q (2017) Trace theorems for some nonlocal function spaces with heterogeneous localization. SIAM J Math Anal 49(2):1621–1644
145. Tian X, Du Q (2020) Asymptotically compatible schemes for robust discretization of parametrized problems with applications to nonlocal models. SIAM Rev 62(1):199–227
146. Toselli A, Widlund O (2006) Domain Decomposition Methods - Algorithms and Theory, vol 34. Springer-Verlag Berlin Heidelberg
147. Trageser J, Seleson P (2019). Anisotropic two-dimensional, plane strain, and plane stress models in classical linear elasticity and bond-based peridynamics. arXiv:1905.12761
148. Trageser J, Seleson P (2020) Bond-based peridynamics: a tale of two Poisson's ratios. J Peridyn Nonlocal Model 2:278–288
149. Wang X, Kulkarni SS, Tabarraei A (2019) Concurrent coupling of peridynamics and classical elasticity for elastodynamic problems. Comput Methods Appl Mech Eng 344:251–275
150. Weinan E, Lu J, Yang JZ (2006) Uniform accuracy of the quasicontinuum method. Physics Review B 74:214115
151. Wildman RA, Gazonas GA (2014) A finite difference-augmented peridynamics method for reducing wave dispersion. Int J Fract 190(1-2):39–52
152. Xu F, Gunzburger M, Burkardt J (2016) A multiscale method for nonlocal mechanics and diffusion and for the approximation of discontinuous functions. Comput Methods Appl Mech Eng 307: 117–143
153. Xu F, Gunzburger M, Burkardt J, Du Q (2016) A multiscale implementation based on adaptive mesh refinement for the nonlocal peridynamics model in one dimension. Multiscale Modeling & Simulation 14(1):398–429
154. Yaghoobi A, Chorzepa MG (2018) Formulation of symmetry boundary modeling in non-ordinary state-based peridynamics and coupling with finite element analysis. Mathematics and Mechanics of Solids 23(8):1156–1176
155. Yang D, He X, Yi S, Deng Y, Liu X (2020) Coupling of peridynamics with finite elements for brittle crack propagation problems. Theoretical and Applied Fracture Mechanics 107:102505
156. You H, Lu XY, Trask N, Yu Y (2020) An asymptotically compatible approach for Neumann-type boundary condition on nonlocal problems. ESAIM: Mathematical Modelling and Numerical Analysis 54(4):1373–1413
157. You H, Yu Y, Kamensky D (2020) An asymptotically compatible formulation for local-to-nonlocal coupling problems without overlapping regions. Comput Methods Appl Mech Eng 366:113038

158. Yu Y, Bargos FF, You H, Parks ML, Bittencourt ML, Karniadakis GE (2018) A partitioned coupling framework for peridynamics and classical theory: Analysis and simulations. Comput Methods Appl Mech Eng 340:905–931
159. Zaccariotto M, Mudric T, Tomasi D, Shojaei A, Galvanetto U (2018) Coupling of FEM meshes with peridynamic grids. Comput Methods Appl Mech Eng 330:471–497
160. Zaccariotto M, Tomasi D, Galvanetto U (2017) An enhanced coupling of PD grids to FE meshes. Mech Res Commun 84:125–135
161. Zheng G, Shen G, Hu P, Xia Y (2020) Coupling approach of isogeometric analysis with non-ordinary state-based peridynamics. European Journal of Mechanics-A/Solids 82:103981